

# Evaluating the assimilation of S5P/Tropomi NRT SO<sub>2</sub> columns and layer height data into the CAMS integrated forecasting system (CY47R1), based on a case study of the 2019 Raikoke eruption

5 Antje Inness<sup>1</sup>, Melanie Ades<sup>1</sup>, Dimitris Balis<sup>3</sup>, Dmitry Efremenko<sup>2</sup>, Johannes Flemming<sup>1</sup>, Pascal Hedelt<sup>2</sup>, Maria-Elissavet Koukouli<sup>3</sup>, Diego Loyola<sup>2</sup>, and Roberto Ribas<sup>1</sup>

<sup>1</sup>European Centre for Medium-Range Weather Forecasts (ECMWF), Shinfield Park, Reading, RG2 9AX, UK.

<sup>2</sup>Deutsches Zentrum für Luft und Raumfahrt (DLR), Institut für Methodik der Fernerkundung (IMF), Oberpfaffenhofen, Germany.

<sup>3</sup>Laboratory of Atmospheric Physics, Aristotle University of Thessaloniki, Greece

10 *Correspondence to:* Antje Inness (antje.inness@ecmwf.int)

## Abstract.

The Copernicus Atmosphere Monitoring Service (CAMS), operated by the European Centre for Medium-Range Weather Forecasts on behalf of the European Commission, provides daily analyses and 5-day forecasts of atmospheric composition, including forecasts of volcanic sulphur dioxide (SO<sub>2</sub>) in near-real time. CAMS currently assimilates total column SO<sub>2</sub>

15 products from the GOME-2 instruments on MetOp-B and -C and the TROPOMI instrument on Sentinel-5P which give information about the location and strength of volcanic plumes. However, the operational TROPOMI and GOME-2 data do not provide any information about the height of the volcanic plumes and therefore some prior assumptions need to be made in the CAMS data assimilation system about where to place the resulting SO<sub>2</sub> increments in the vertical. In the current operational CAMS configuration, the SO<sub>2</sub> increments are placed in the mid-troposphere, around 550 hPa or 5 km. While this 20 gives good results for the majority of volcanic emissions, it will clearly be wrong for eruptions that inject SO<sub>2</sub> at very different altitudes, in particular exceptional events where part of the SO<sub>2</sub> plume reaches the stratosphere.

A new algorithm, developed by DLR for GOME-2 and TROPOMI and optimized in the frame of the ESA-funded Sentinel-5P Innovation–SO<sub>2</sub> Layer Height Project, the Full-Physics Inverse Learning Machine (FP\_ILM) algorithm, retrieves SO<sub>2</sub>

25 layer height from TROPOMI in NRT in addition to the SO<sub>2</sub> column. CAMS is testing the assimilation of these products, making use of the NRT layer height information to place the SO<sub>2</sub> increments at a retrieved altitude. Assimilation tests with the TROPOMI SO<sub>2</sub> layer height data for the Raikoke eruption in June 2019 show that the resulting CAMS SO<sub>2</sub> plume heights agree better with IASI plume height data than operational CAMS runs without the TROPOMI SO<sub>2</sub> layer height information and that making use of the additional layer height information leads to improved SO<sub>2</sub> forecasts than when using 30 the operational CAMS configuration. Including the layer height information leads to higher modelled TCSO<sub>2</sub> values in better agreement with the satellite observations. However, the plume area and SO<sub>2</sub> burden are generally overestimated in the CAMS analysis also when LH data are used. The main reason for this overestimation is the coarse horizontal resolution used in the minimisations. By assimilating the SO<sub>2</sub> layer height data the CAMS system can predict the overall location of the 35 Raikoke SO<sub>2</sub> plume up to 5 days in advance for about 20 days after the initial eruption, which is better than with the operational CAMS configuration (without prior knowledge of the plume height) where the forecast skill reduces much more for longer forecast lead-times.

## 1 Introduction

40 Volcanoes can cause serious disruptions for society, not just for people living near them, but also further afield when ash and sulphur dioxide ( $\text{SO}_2$ ) emitting from highly explosive eruptions reach the upper troposphere or stratosphere, above the clouds, and therefore are transported over vast distances by the prevailing winds. Ash and  $\text{SO}_2$  are a serious concern for the aviation industry, reducing visibility and in severe cases can lead to engine failure or cause permanent damage to aircraft engines (Prata et al., 2019). The immediate danger to the aircraft comes mainly from the emitted ash, although  $\text{SO}_2$  is also an  
45 aviation hazard, potentially causing long-term damage via corrosion and sulfidation of the engines (Schmidt et al., 2014). If sufficient  $\text{SO}_2$  is diffused into the aircraft cabin this could potentially lead to respiratory problems for passengers and crew. Planes therefore try to avoid volcanic plumes and after the 2010 eruption of the Icelandic Eyjafjallajökull volcano (e.g. Stohl et al., 2011; Dacre et al., 2011; Thomas and Prata, 2011) European air traffic was grounded for several days. Forecasts of the location and the altitude of volcanic  $\text{SO}_2$  or ash plumes can therefore provide important information for the aviation industry.  
50 Satellite retrievals of volcanic ash and  $\text{SO}_2$  can help to track volcanic plumes, as done by the Support to Aviation Control Service (sacs.aeronomie.be; Brenot et al., 2014) and the EUNADICS (European Natural Airborne Disaster Information and Coordination System for Aviation) prototype Early Warning System (Brenot et al., 2021). These services, as well as plume dispersion modelling (e.g. de Leeuw et al., 2021; Harvey and Dacre, 2016), are used by the Volcanic Ash Advisory Centres (VAACs) to advise civil aviation authorities in case of volcanic eruptions. While  $\text{SO}_2$  is often used as a proxy for ash, the  
55  $\text{SO}_2$  and ash plumes can be located at different altitudes and be transported in different directions as was the case for the Icelandic Grímsvötn eruption in 2011 (Moxnes et al., 2013, Prata et al., 2017).

The Copernicus Atmosphere Monitoring Service (CAMS), operated by the European Centre for Medium-Range Weather Forecasts (ECMWF) on behalf of the European Commission, provides daily analyses and 5-day forecasts of atmospheric  
60 composition, including forecasts of volcanic  $\text{SO}_2$  in near-real time (NRT). Since the CAMS forecast system runs within 3 hours of the observations being taken, information about volcanic  $\text{SO}_2$  emission strength and the altitude of  $\text{SO}_2$  plumes is usually not available, with only the total column-integrated  $\text{SO}_2$  amount (TCSO<sub>2</sub>) able to be provided to adjust the model's predictions. CAMS uses the method described in Flemming and Inness (2013) in its operational NRT system to routinely assimilate NRT TCSO<sub>2</sub> data from the Global Ozone Monitoring Experiment-2 (GOME-2) instruments produced by  
65 Eumetsat's Satellite Application Facility on Atmospheric Composition Monitoring (ACSAF) and from the Sentinel-5P Tropospheric Monitoring Instrument (TROPOMI) provided by the European Space Agency (ESA). Both products are derived using retrievals developed by the German Aerospace Centre (DLR) and give information about the emitted volcanic  $\text{SO}_2$  and the horizontal location in NRT but do not provide any information about the altitudes of the volcanic plumes. Prior assumptions therefore need to be made in the CAMS data assimilation system about where in the vertical the resulting  $\text{SO}_2$   
70 increments should be placed. In the absence of NRT height information, the default is to place the  $\text{SO}_2$  increments in the mid-troposphere, around 550 hPa or 5 km. Although clearly a simplified approach, the method is a reasonable approximation to the real situation, using the data assimilation procedure as a mid-tropospheric  $\text{SO}_2$  source in areas of elevated volcanic TCSO<sub>2</sub>. The  $\text{SO}_2$  analysis field will then be transported by the model's prevailing winds and thereby result in quite realistic volcanic  $\text{SO}_2$  plumes. While this method produces good results for a large number of volcanic eruptions that inject  $\text{SO}_2$  into  
75 the mid-troposphere, it will clearly be wrong for eruptions that inject  $\text{SO}_2$  at very different altitudes, in particular for the most explosive events where part of the  $\text{SO}_2$  reaches the stratosphere. In those cases, the CAMS system will not be able to forecast the  $\text{SO}_2$  transport well, because the model  $\text{SO}_2$  plume will be located at the wrong altitude where the prevailing winds might transport the  $\text{SO}_2$  in the wrong direction or height. The availability and use of NRT information about the altitude of the volcanic plumes would greatly improve the quality of the CAMS  $\text{SO}_2$  analysis and subsequent forecasts.

80

For hindcasts of volcanic eruptions with a system that does not run in NRT it is easier to make use of better injection height information. In this case, observations about injection height and emission strength might be available. Furthermore, CAMS

can run an ensemble of SO<sub>2</sub> tracers emitted at different altitudes and determine the best altitude and emission strength from comparisons of the resulting model fields with the available TCSO<sub>2</sub> observations, using a method described in Flemming and 85 Inness (2013). The parameters (plume height and emission flux) derived in this way can subsequently be used to provide a volcanic SO<sub>2</sub> source term in the CAMS forecast model and can also be used in the data assimilation system to modify the SO<sub>2</sub> background error standard deviation to peak at the corresponding model level. However, this is not possible in NRT.

A new algorithm, developed by DLR for GOME-2 and adapted to TROPOMI, which is currently being optimized in the 90 frame of the ESA-funded Sentinel-5P (S5P) Innovation–SO<sub>2</sub> Layer Height Project (S5P+I: SO<sub>2</sub>LH), the Full-Physics Inverse Learning Machine (FP\_ILM) algorithm (Hedelt et al., 2019), retrieves SO<sub>2</sub> layer height (LH) information from TROPOMI in NRT in addition to the SO<sub>2</sub> column. This is different from the operational ESA NRT TROPOMI product which does not 95 provide plume height information. CAMS is testing the assimilation of the FP\_ILM data, making use of the NRT LH information. In this paper we document the current use of the operational TCSO<sub>2</sub> data in the CAMS data assimilation system, present results from assimilation tests with the FP\_ILM TROPOMI SO<sub>2</sub> LH data for the eruption of the Raikoke volcano in June 2019 and show that making use of the NRT LH information leads to improved SO<sub>2</sub> analyses and in particular SO<sub>2</sub> forecasts.

This paper is structured in the following way. Section 2 describes the SO<sub>2</sub> datasets used in this study and Section 3 describes 100 the CAMS model and SO<sub>2</sub> data assimilation setup. Section 4 presents the results from the assimilation of TROPOMI data for eruption of Raikoke in June 2019, including sensitivity studies to evaluate choices made for the SO<sub>2</sub> background errors, and evaluates the quality of the resulting SO<sub>2</sub> analyses and forecasts with and without LH information. Section 5 presents the conclusions.

## 2 Datasets

105 The SO<sub>2</sub> satellite data currently used in the CAMS NRT system are the operational TCSO<sub>2</sub> products from TROPOMI on S5P produced by ESA and from the GOME-2 instruments on MetOp-B and MetOp-C produced by Eumetsat's ACSAF. These data come with a volcanic flag, i.e. the data producers mark the pixels that are affected by volcanic SO<sub>2</sub>, and only pixels that are flagged as volcanic are assimilated in the CAMS system. Using TROPOMI in addition to GOME-2 has two advantages: 110 (1) TROPOMI has better spatial coverage and a lower detection limit than GOME-2 and (2) because TROPOMI has a different overpass time (9.30 UTC for MetOp, 13.30 UTC for S5P) using both instruments improves the chances of having an overpass over a volcano when an eruption happens or shortly afterwards.

### 2.1 NRT TROPOMI TCSO<sub>2</sub> data

TROPOMI on board the S5P satellite provides high-resolution spectral measurements in the ultraviolet (UV), visible (Vis), 115 near infrared and shortwave-infrared parts of the spectrum, allowing several atmospheric trace gases to be retrieved, including SO<sub>2</sub> from the UV–Vis part of the spectrum. The horizontal resolution of TROPOMI for the UV-Vis is 5.5 km x 3.5 km (7 km x 3.5 km before 6 August 2019) with daily global coverage. The theoretical baseline for the operational TROPOMI SO<sub>2</sub> retrieval is described in Theys et al. (2017) and further information can be found in Algorithm Theoretical Basis Document (ATBD), Product User Manual (PUM) and readme files available from the TROPOMI website (http://www.tropomi.eu/documents/). The atmospheric SO<sub>2</sub> vertical column density is retrieved in three fitting windows 120 (312–326 nm, 325–335 nm and 360–390 nm) using a Differential Optical Absorption Spectroscopy (DOAS) method (Platt and Stutz, 2008; Platt, 2017), in which the slant SO<sub>2</sub> column is retrieved and converted into vertical columns by using air mass factors. The log-ratio of the observed UV-visible spectrum of radiation backscattered from the atmosphere and an

observed reference spectrum are used to derive a slant column density, which represents the SO<sub>2</sub> concentration integrated along the mean light path through the atmosphere. This is performed by fitting SO<sub>2</sub> absorption cross-sections to the measured reflectance in a given spectral interval. In a second step, slant columns are corrected for possible biases. Finally, the slant columns are converted into vertical columns by means of air mass factors obtained from radiative transfer calculations, accounting for the viewing geometry, clouds, surface properties and prior SO<sub>2</sub> vertical profile shapes. A volcano activity detection algorithm going back to Brenot et al. (2014) is used to identify elevated SO<sub>2</sub> values from volcanic eruptions (see Table 1). CAMS only assimilates SO<sub>2</sub> pixels that have flag values of 1 (enhanced SO<sub>2</sub> detection) or 2 (enhanced SO<sub>2</sub> detection in vicinity of known volcano). Furthermore, only TROPOMI SO<sub>2</sub> pixels with values greater than 5 DU are assimilated in the operational CAMS system to avoid assimilating SO<sub>2</sub> from outgassing volcanoes which are covered by SO<sub>2</sub> emissions in the CAMS model. The TROPOMI SO<sub>2</sub> data are super-obbed, i.e. in a pre-processing step area means are created by averaging all data (observation values as well as errors) in a model grid box to the model resolution (TL511, about 40km). These super-observations are then used in the CAMS system without further thinning.

135

The DOAS vertical column SO<sub>2</sub> retrieval requires an assumption for a prior SO<sub>2</sub> profile to convert the slant columns into vertical columns. Since this profile shape is generally not known at the time of the observation and it is also not known whether the observed SO<sub>2</sub> is of volcanic origin or from pollution (or both) the TROPOMI algorithm calculates four vertical columns for different hypothetical SO<sub>2</sub> profiles. One vertical column is provided for anthropogenic SO<sub>2</sub> with the prior SO<sub>2</sub> profile taken from the TM5 CTM and three for volcanic scenarios assuming the SO<sub>2</sub> is either located in the boundary layer, 140 in the mid-troposphere (around 7 km) or in the stratosphere (around 15 km). These volcanic prior profiles are box profiles of 1 km thickness, located at the corresponding altitudes. The NRT CAMS system uses the mid-troposphere product. TROPOMI SO<sub>2</sub> data are provided with averaging kernels based on the prior hypothetical SO<sub>2</sub> profiles (i.e. the 1 km box profiles centred around the assumed SO<sub>2</sub> altitude for the volcanic columns). However, as these do not provide information 145 about the real altitude of a specific volcanic plume they are not used in the CAMS system. More information about the NRT TROPOMI SO<sub>2</sub> retrieval can be found in the TROPOMI ATBD. For the TROPOMI data (and also the other SO<sub>2</sub> products used in this paper) observation errors as given by the data providers are used within the CAMS data assimilation system.

Flag value	Description
0	No detection
1	Enhanced SO <sub>2</sub> detection
2	Enhanced SO <sub>2</sub> detection in vicinity of known volcano
3	Enhanced SO <sub>2</sub> in vicinity of anthropogenic source
4	Enhanced SO <sub>2</sub> in SAA or for SZA>70°

150 **Table 1: Volcanic SO<sub>2</sub> flags provided for the TROPOMI SO<sub>2</sub> products. The same flags are also used for TROPOMI SO<sub>2</sub>LH data and GOME-2C GPD4.9 SO<sub>2</sub> data.**

## 2.2 FP\_ILM NRT TROPOMI Layer Height data

Hedelt et al. (2019) have developed an algorithm called 'Full-Physics Inverse Learning Machine' (FP\_ILM) for the retrieval 155 of the SO<sub>2</sub> LH based on Sentinel-5 precursor/TROPOMI data using a coupled Principal Component Analysis and Neural Network approach including regression. This algorithm is an improvement of the original FP\_ILM algorithm developed by Efremenko et al. (2017) for the retrieval of the SO<sub>2</sub> LH based on GOME-2 data using a Principal Component Regression technique. Recently, this algorithm has also been adapted to retrieve SO<sub>2</sub> LH data from the Ozone Monitoring Instrument

(OMI) on the Aura satellite (Fedkin et al., 2021). Furthermore, the FP\_ILM algorithm has been used for the retrieval of ozone profile shapes (Xu et al., 2017) and the retrieval of surface properties accounting for bidirectional reflectance distribution function effects (Loyola et al., 2020). In general, the FP\_ILM algorithm creates a mapping between the spectral radiance and atmospheric parameter using machine learning methods. The time-consuming training phase of the algorithm using radiative transfer model calculations is performed off-line, and only the inversion operator has to be applied to satellite measurements which makes the algorithm extremely fast, and it can thus be used in NRT processing environments. SO<sub>2</sub> LH is retrieved in NRT from TROPOMI UV earthshine spectra in the wavelength range 311-335 nm with an accuracy of better than 2 km for SO<sub>2</sub> columns greater than 20 DU. For low SO<sub>2</sub> columns, high-altitude layer heights cannot be retrieved and the retrieval is biased towards low layer heights (Hedelt et al., 2018). Therefore, the use of the data in the CAMS system is restricted to values > 20 DU. More details about the retrieval algorithm can be found in Hedelt et al. (2018) and Koukouli et al. (2021). Koukouli et al. (2021) compared the S5P LH data with IASI observations for the 2019 Raikoke, the 2020 Nishinoshima and the 2021 La Soufrière-St Vincent eruptive periods and found good agreement with a mean difference of  $\sim 0.5 \pm 3$  km, while for the 2020 Taal eruption, a larger difference of between 3 and  $4 \pm 3$  km was found. In this paper we use v3.1 of the FP\_ILM SO<sub>2</sub> LH products.

### 2.3 NRT GOME-2 TCSO<sub>2</sub> data

GOME-2 (Munro et al., 2016) on board the MetOp-A, -B and -C satellites measures in the UV and Vis part of the spectrum (240-790 nm). MetOp-B and -C have a swath of 1920 km at 40 km x 80 km ground pixel resolution, while MetOp-A has a narrower swath of 960 km at 40 km x 40 km. Global coverage with GOME-2 is achieved within 1.5 days. The GOME-2 measurements allow for the retrieval of ozone and a range of atmospheric trace gases, including SO<sub>2</sub> which is retrieved with the GOME Data Processor (GDP) developed by DLR and operationally provided by the EUMETSAT's ACSAF that uses a DOAS method. GDP4.8 is used for GOME-2A and GOME-2B (with a fitting window from 315-326 nm) and GDP4.9 for GOME-2C (with a fitting window of 312-326 nm to include the strong SO<sub>2</sub> line at 313 nm). Input parameters for the DOAS fit include the absorption cross section of SO<sub>2</sub> and the absorption cross sections of interfering gases, ozone and NO<sub>2</sub>, and a correction is made in the DOAS fit to account for the ring effect (rotational Raman scattering). An empirical interference correction is applied to the SO<sub>2</sub> slant column values to reduce the interference from ozone absorption (Rix et al., 2012). To reduce the interference from ozone absorption, the retrieval includes the fitting of two pseudo ozone cross-sections following the approach of Puķīte et al. (2010). As in the case for the TROPOMI dataset, a volcano activity detection algorithm is used to identify elevated SO<sub>2</sub> values from volcanic eruptions. Such flags were implemented in GDP4.8 (see Table 2) and further improved in GDP4.9 to use the same flagging as for TROPOMI (see Table 1). CAMS only assimilates the GOME-2 SO<sub>2</sub> data that are flagged as volcanic (value=1 for GDP4.8; value=1 or 2 for GDP4.9) and assimilates GOME-2B and GOME-2C in the NRT system operational in 2021. The GOME-2 data are used at the satellite resolution which is similar to the resolution of the CAMS model used in this paper. In this paper only SO<sub>2</sub> data from GOME-2B are used.

Flag value	Description
0	No detection
1	Elevated SO <sub>2</sub> value due to a volcanic SO <sub>2</sub> plume
2	Elevated SO <sub>2</sub> value in a region with known increased background level (either anthropogenic pollution or SAA region)

Table 2: Volcanic SO<sub>2</sub> flags provided for the GDP4.8 GOME-2A and -2B SO<sub>2</sub> products.

195 **2.4 IASI SO<sub>2</sub> plume altitude data**

The Infrared Atmospheric Sounding Instrument (IASI) is flying on board of EUMETSAT's MetOp-A (since 2006), MetOp-B (since 2012) and MetOp-C (since 2017) satellite platforms (Clerbaux et al., 2015). The instruments measure the upwelling radiances in the thermal infrared spectral range extending from 645 to 2760 cm<sup>-1</sup>, with high radiometric quality, 0.5 cm<sup>-1</sup> spectral resolution. A total of 120 views are collected over a swath of  $\sim$  2200 km using a stare-and-stay mode of 30 arrays of 200 4 individual elliptical pixels, each of which is 12 km diameter at nadir, increasing at the larger viewing angles. IASI provides global monitoring of total ozone, carbon monoxide, methane, ammonia, nitric acid and SO<sub>2</sub>, among others atmospheric constituents.

The IASI/MetOp SO<sub>2</sub> columnar data are operationally provided by the EUMETSAT's ACSAF. In Clarisse et al. (2012) a 205 novel algorithm for the sounding of volcanic SO<sub>2</sub> plumes above  $\sim$  5 km altitude was presented and applied to IASI observations. The algorithm is able to view a wide variety of total column ranges (from 0.5 to 5000 D.U.), exhibits a low theoretical uncertainty (3–5 %) and near real time applicability which was demonstrated for the recent eruptions of Sarychev in Russia, Kasatochi in Alaska, Grimsvötn in Iceland, Puyehue-Cordon Caulle in Chile and Nabro in Eritrea (Tournigand et al., 2020.) A validation of this algorithm on the Nabro eruption observations using forward trajectories and 210 CALIOP/CALIPSO space-born lidar coincident measurements is presented in Clarisse et al. (2014) where the expansion of the algorithm to also provide SO<sub>2</sub> plume altitudes is further described. The IASI/MetOp SO<sub>2</sub> ACSAF product includes five SO<sub>2</sub> column data at assumed layer heights of 7, 10, 13, 16 and 25 km, as well as a retrieved best estimate for the SO<sub>2</sub> plume altitude and associated SO<sub>2</sub> column. Note that the SO<sub>2</sub> plume altitudes provided by this algorithm are quantized every 0.5km. This dataset is publicly available from [https://iasi.aeris-data.fr/SO2\\_iasi\\_a\\_arch/](https://iasi.aeris-data.fr/SO2_iasi_a_arch/).

215

For the requirements of the validation against the CAMS experiments, all available IASI SO<sub>2</sub> plume altitude data for the Raikoke volcano 2019 eruption were gridded onto a 1x1° grid at 3h intervals per day. The equivalent CAMS SO<sub>2</sub> plume altitude, i.e. the altitude where the maximum SO<sub>2</sub> load occurs in the CAMS SO<sub>2</sub> profiles, was chosen for the collocations. In the case where two CAMS altitudes provided the same SO<sub>2</sub> load, the mean was assigned as the CAMS SO<sub>2</sub> plume altitude.

220

### 3 CAMS global integrated forecasting and data assimilation system

#### 3.1 CAMS volcanic SO<sub>2</sub> plume forecasting system

The chemical mechanism of ECMWF's Integrated Forecast System (IFS) is a modified and extended version of the Carbon Bond 2005 chemistry scheme (CB05, Yarwood et al. 2005) chemical mechanism for the troposphere, as also implemented in 225 the chemical transport model (CTM) TM5 (Huijnen et al., 2010). CB05 is a tropospheric chemistry scheme with 57 species and 131 reactions. The chemistry module of the IFS is documented in more detail in Flemming et al. (2015) and Flemming et al. (2017) and more recent updates in Inness et al. (2019). The CB05 chemistry scheme is coupled to the AER aerosol bulk scheme (Remy et al. 2019) for the simulation of sulphate, nitrate and ammonium aerosols. More up-to-date information is available from [atmosphere.copernicus.eu](http://atmosphere.copernicus.eu). In the original version of the volcanic SO<sub>2</sub> plume forecasting system described by 230 Flemming and Inness (2013), there was a dedicated "volcanic SO<sub>2</sub> tracer", with oxidation based on a simple fixed timescale approach. By contrast, in the progression of the volcanic SO<sub>2</sub> system described here, the volcanic SO<sub>2</sub> emissions, and data assimilation of SO<sub>2</sub>, is applied to the SO<sub>2</sub> tracer within the CB05 chemistry scheme (Flemming et al., 2015), with oxidation to sulphate aerosol occurring, based on the kinetics specified in the chemistry scheme. The main SO<sub>2</sub> loss in the coupled

chemistry-aerosol system is the conversion to sulfuric acid. There are two pathways for this (i) in the gas phase via the 235 hydroxyl radical (OH) and (ii) in clouds (aqueous phase). Pathway (i) via OH is the main pathway in the stratosphere. Heterogenous conversion on ash particles, is not directly modelled in the IFS. Other loss processes are wet deposition and surface dry deposition. As described in Flemming et al. (2015) the IFS uses a semi-Lagrangian advection scheme. Since the semi-Lagrangian advection does not formally conserve mass, a global mass fixer is applied to the chemical tracers, including to the SO<sub>2</sub> tracer, and a proportional mass fixer as described in Diamantakis and Flemming (2014) was used for the runs 240 presented in this paper. More details about the CB05 chemistry scheme can be found in Flemming et al. (2015, 2017), Remy et al. (2018) and Huijnen et al. (2019).

The model version used in this paper is based on the IFS model cycle 47R1 (CY47R1, [www.ecmwf.int/en/forecasts/documentation-and-support/changes-ecmwf-model](http://www.ecmwf.int/en/forecasts/documentation-and-support/changes-ecmwf-model)), which was the operational CAMS cycle from 6 October 2020 to 18 May 2021. In CY47R1, the CAMS system uses the CAMS-GLOBANTv4.2 anthropogenic 245 emissions (Granier et al., 2019) which include anthropogenic SO<sub>2</sub>, as well as a climatology of SO<sub>2</sub> outgassing volcanic emissions based on satellite data (Carn et al., 2016). Further updates relative to the previous version (CY46R1) are

- change to Global Fire Assimilation System (GFAS) v1.4 biomass-burning emissions
- the exclusion of agricultural waste burning from CAMS\_GLOB\_ANT to avoid double-counting with GFAS
- improved diurnal cycle and vertical profile for anthropogenic emissions
- introduction of Hybrid Linear Ozone (HLO) scheme, a Cariolle-type linear parameterisation of stratospheric ozone 250 chemistry using the multi-year mean of the CAMS reanalysis as mean state
- updated dust source function, which reduces the overestimation of dust in the Sahara, Middle East and other regions, and restores missing dust over Australia
- new sea-salt emission scheme based on Albert et al. (2016), which provides better agreement with measured sea- 255 salt size distribution
- revised coefficients in UV processor, based on ATLAS3 spectrum.

### 3.2 CAMS data assimilation system

The IFS uses an incremental four-dimensional variational (4D-Var) data assimilation system (Courtier et al. 1994). In the 260 CAMS 4D-Var a cost function that measures the differences between the model fields and the observations is minimized to obtain the best possible forecast through the length of the assimilation window by adjusting the initial conditions. SO<sub>2</sub> is one of the atmospheric composition fields that is included in the control vector and minimized together with the meteorological control variables in the CAMS system (Inness et al., 2015, Flemming and Inness, 2013). The current operational CAMS configuration uses a weak constraint formulation of 4D-Var which includes a model error term for the meteorological 265 variables (Laloyaux et al., 2020) that corrects mainly the stratospheric temperature bias and also improves slightly the stratospheric winds. In the CAMS 4D-Var system, the control variables are the initial conditions at the beginning of the assimilation window, with the aim of providing the best initial conditions for the subsequent forecast. The background error covariance matrix in the ECMWF data assimilation system is given in a wavelet formulation (Fisher 2004, 2006). This allows both spatial and spectral variations of the horizontal and vertical background error covariances. The CAMS 270 background errors are constant in time. The horizontal resolution of the NRT CAMS 2021 operational system as well as that of the data assimilation experiments presented in this paper is approximately 40 km, corresponding to a triangular truncation of TL511 or a reduced Gaussian grid with a resolution of N256 (more information can be found at <https://confluence.ecmwf.int/display/FCST/Gaussian+grids>). The operational CAMS system uses two minimisations (the so-called inner loops) at reduced horizontal resolution, currently at TL95 and TL159 corresponding to horizontal resolutions of 275 about 210 km and 125 km. This means that wavenumbers up to 95/159 can be represented in the wavelet formulation for the

background errors. For the experiments presented in this paper, slightly higher horizontal resolutions of TL159/TL255 were used for the inner loops (corresponding to about 125 and 80 km, respectively). The CAMS model and data assimilation system has 137 model levels in the vertical, between the surface and 0.01 hPa and uses a 12-hour 4D-Var configuration with assimilation windows from 3 to 15 UTC and from 15-3 UTC.

280 **3.2.1 CAMS NRT TCSO<sub>2</sub> assimilation configuration (baseline configuration)**

The SO<sub>2</sub> data assimilated in the CAMS NRT configuration are total column values. To calculate the model equivalent of the observations the CAMS SO<sub>2</sub> field is interpolated to the time and location of the measurements and the CAMS SO<sub>2</sub> columns are calculated as a simple vertical integral between the surface and the top of the atmosphere. While the background error statistics for most of the atmospheric composition fields (Inness et al., 2015) were either calculated with the National 285 Meteorological Center (NMC) method (Parrish and Derber, 1992) or from an ensemble of forecast differences (following a method described by Fisher and Andersson, 2001), the background errors for SO<sub>2</sub> are prescribed by an analytical vertical standard deviation profile and horizontal correlations. SO<sub>2</sub> observations are currently only assimilated in the CAMS system in the event of volcanic eruptions. An NMC or ensemble approach would not give useful SO<sub>2</sub> background error statistics in these cases as the forecast model does not have information about individual volcanic eruptions, even though it does include 290 emissions from outgassing volcanoes. SO<sub>2</sub> background error standard deviations calculated with the NMC or ensemble methods peak near the surface where anthropogenic SO<sub>2</sub> concentrations are largest and will hence lead to the largest analysis increments near the surface. Therefore, for the assimilation of volcanic SO<sub>2</sub> data, background error statistics for SO<sub>2</sub> were constructed by prescribing a background error standard deviation profile that is a delta function and peaks in the mid troposphere around model level 98 (about 550 hPa) in the 137 level model version, corresponding to an SO<sub>2</sub> plume height of 295 about 5 km (see blue profile in Figure 1).

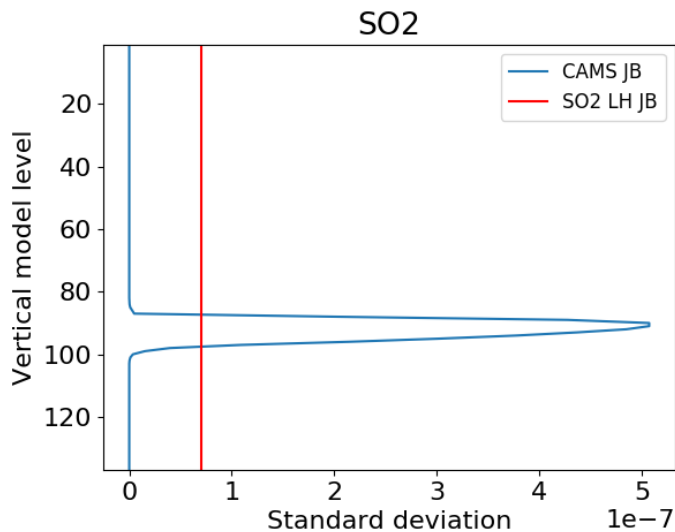


Figure 1: Vertical profile of SO<sub>2</sub> background error standard deviation in kg/kg used in the operational CAMS configuration (blue) and for the main LH experiment (red, LHexp). The y-axis shows model levels. Level 1 is the top of the atmosphere, level 137 the surface.

300

The SO<sub>2</sub> wavelet file in the NRT CAMS configuration (also called baseline configuration in this paper) is formed of diagonal vertical wavenumber correlation matrices, with the value on the diagonal controlled by a horizontal Gaussian correlation function with a standard deviation of 250 km and a globally constant vertical standard deviation profile. The values of the elements on the diagonal of the vertical correlation matrix are the same at every level but vary for each 305 wavenumber. If TCSO<sub>2</sub> data are assimilated the largest correction to the model's background will be applied where the

background errors are largest, i.e. in the mid-troposphere around 550 hPa. The CAMS SO<sub>2</sub> analysis is univariate, i.e. there are no cross correlations between SO<sub>2</sub> background errors and the other atmospheric composition control variables.

### 3.2.2 Data assimilation configuration for TCSO<sub>2</sub> LH data

310 If information about the altitude of the volcanic SO<sub>2</sub> layer is known in NRT a different approach can be followed. In this case, we use a background error standard deviation profile that is constant in height (e.g. red line in Fig. 1) and calculate the SO<sub>2</sub> column not between the surface and the top of the atmosphere, but between the pressure values that correspond to the bottom and the top of the retrieved volcanic SO<sub>2</sub> layer. The depth of this layer is currently set in the FP\_ILM product as 2 km, which corresponds to the uncertainty of the retrieved layer height. This approach mimics the procedure of using  
315 TROPOMI SO<sub>2</sub> averaging kernels which are box profiles, but for the retrieved layer and not an assumed hypothetical volcanic SO<sub>2</sub> profile (see TROPOMI SO<sub>2</sub> ATBD, <http://www.tropomi.eu/documents/>). One limitation of this method is that the SO<sub>2</sub> LH product gives the plume altitude with an accuracy of 2 km, but does not give a value for the lower vertical boundary of the SO<sub>2</sub> plume, and for a thick plume part of the SO<sub>2</sub> loading could be missed in the calculation of the model equivalent. However, as the model's background SO<sub>2</sub> concentrations in the free troposphere are low this should not be a big  
320 issue in the column calculation. Also, some vertical variation of the SO<sub>2</sub> loading will result from assimilating observations with varying plume altitudes for larger volcanic plumes that are not uniform in height everywhere, and Figure 3 below shows that this is indeed the case for the Raikoke eruption. Results from sensitivity studies regarding the choice of the constant background error standard deviation value are given below in Section 4.2.

## 325 4. Assimilation of TROPOMI TCSO<sub>2</sub> data for 2019 Raikoke eruption

### 4.1 Raikoke eruption June 2019

The Raikoke volcano, located on the Kuril Islands south of the Kamchatka peninsula, erupted around 18 UTC on 21 June 2019 and emitted SO<sub>2</sub> and ash in a series of explosive events until about 6 UTC on 22 July. The SO<sub>2</sub> and ash plume rose to around 8-18 km (Muser et al., 2020; Grebennikov et al., 2020) meaning a considerable amount of the SO<sub>2</sub> reached the  
330 stratosphere. The volcanic cloud was transported around much of the northern hemisphere, was observed by TROPOMI and GOME-2 for about a month and was also observed with ground-based measurements (Vaughan et al., 2021; Grebennikov et al., 2020) and other satellites (Muser et al., 2020). Figure 2 shows the TCSO<sub>2</sub> burden from the Raikoke eruption as calculated from NRT TROPOMI and GOME-2B data. All the TCSO<sub>2</sub> satellite data available during a 12-hour assimilation window were gridded onto a 1°x1° degree grid and the area of all grid cells with SO<sub>2</sub> values greater than the listed threshold  
335 values was calculated. For a threshold of 1 DU the SO<sub>2</sub> burdens from TROPOMI and GOME-2B were around 1.5 Tg and 1.1 Tg, respectively. These values agree with findings by de Leeuw et al. (2021) and make the eruption the largest since the eruption of the Nabro volcano in 2011 (de Leeuw et al., 2021; Goitom et al., 2015; Clarisse et al., 2014). The 'dip' in the TROPOMI SO<sub>2</sub> burden after the initial peak is an artefact that results from missing observations in the TROPOMI NRT data on 25 June 2019 in the area of highest SO<sub>2</sub> values (also visible in Figure 9c2 below).

340

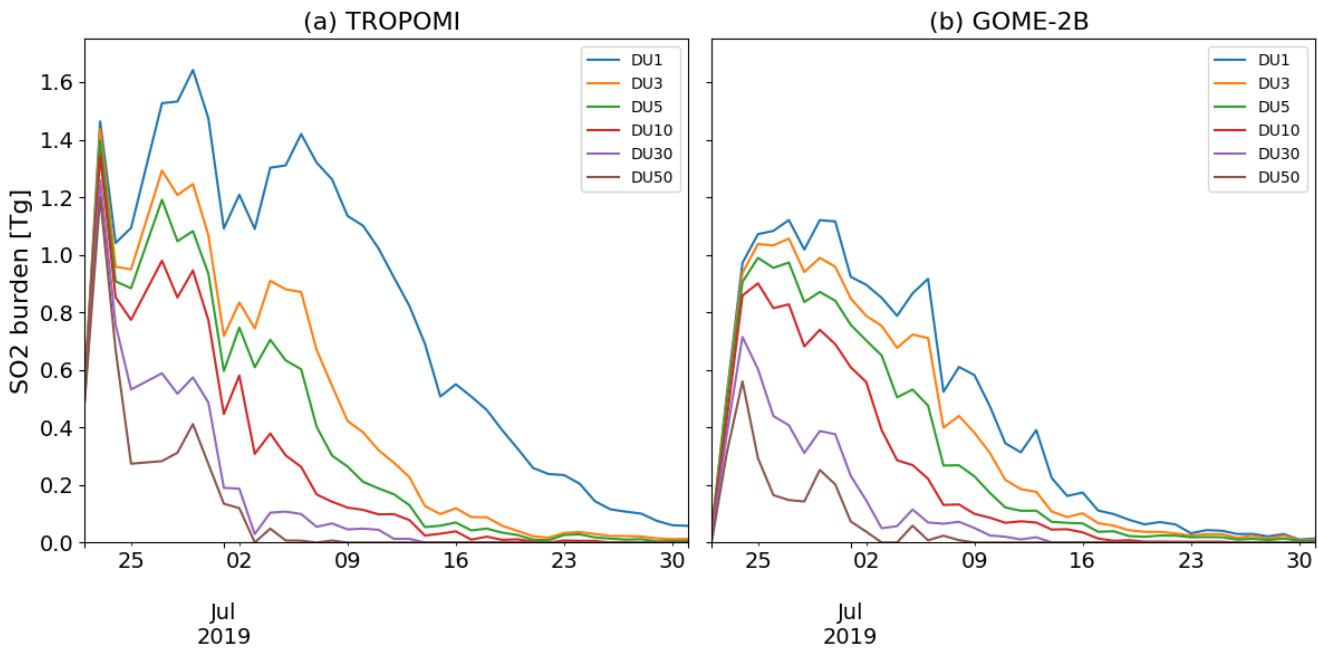


**Figure 2:** SO<sub>2</sub> burden (in Tg) from TROPOMI (left) and GOME-2B (right) from 22 June to 31 July 2031. The values are calculated by gridding the data on a  $1^\circ \times 1^\circ$  grid and selecting the grid cells with TCSO<sub>2</sub> values greater than thresholds of 1, 3, 5, 10, 30 and 50 DU in the area 30–90°N.

345

Figure 3 shows a timeseries of the SO<sub>2</sub> LH information from the TROPOMI LH product for the Raikoke plume. It shows that volcanic SO<sub>2</sub> can be detected and the SO<sub>2</sub> LH information retrieved for about 3 weeks after the eruption. The bulk of the SO<sub>2</sub> was located above 300 hPa, (about 9 km) with a considerable amount above 200 hPa (about 12 km). This is considerably higher than the 550 hPa that is assumed as the plume location in the CAMS operational (baseline) 350 configuration. Large TCSO<sub>2</sub> values (>100 DU) were observed in the first days after the eruption.

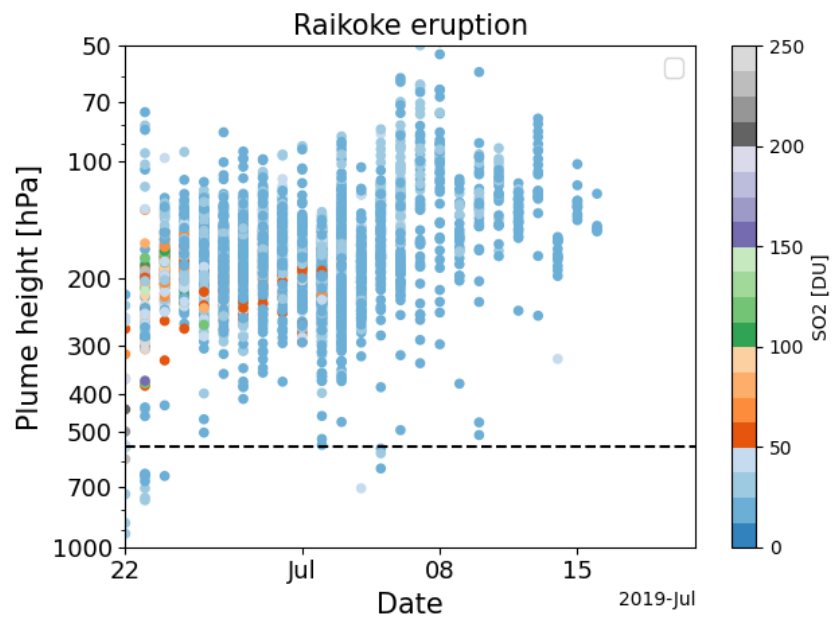


**Figure 3:** Timeseries of the height of the Raikoke volcanic plume (averaged over 30–90°N) in hPa from TROPOMI SO<sub>2</sub> LH data from 22 June to 21 July 2019. The colours show the corresponding TCSO<sub>2</sub> values in DU. The dashed horizontal line at 550 hPa shows the altitude where the CAMS baseline configuration places the maximum SO<sub>2</sub> increment.

355

## 4.2 Sensitivity studies for assimilation of TCSO<sub>2</sub> data

Several data assimilation experiments were run for the period 22 June to 21 July 2019 to test the assimilation of the SO<sub>2</sub> LH data and to compare the results with the CAMS baseline configuration, listed in Table 3. The baseline experiment (BLexp)

360

Experiment Abbreviation	Experiment ID, DOI	Assimilated SO <sub>2</sub> data	Bg-error stdv [kg/kg]	Bg-error hcor [km]	Resolution of minimisations
BLexp	hhu5, <a href="https://doi.org/10.21957/cygt-xf49">10.21957/cygt-xf49</a>	S5P NRT > 5DU	CAMS (see Fig. 2)	250	TL159, TL255
LHexp	hgze, <a href="https://doi.org/10.21957/qfam-7474">10.21957/qfam-7474</a>	S5P LH > 20DU	0.7e <sup>-7</sup>	100	TL159, TL255
LH50	hhbu, <a href="https://doi.org/10.21957/zpdt-f079">10.21957/zpdt-f079</a>	S5P LH > 20DU	1e <sup>-7</sup>	50	TL159, TL255
LH100	hhtm, <a href="https://doi.org/10.21957/jraa-s174">10.21957/jraa-s174</a>	S5P LH > 20DU	1e <sup>-7</sup>	100	TL159, TL255
LH250	hhtn, <a href="https://doi.org/10.21957/ddxs-2v95">10.21957/ddxs-2v95</a>	S5P LH > 20DU	1e <sup>-7</sup>	250	TL159, TL255
LH1.4	hgz7, <a href="https://doi.org/10.21957/81bh-7h58">10.21957/81bh-7h58</a>	S5P LH > 20DU	1.4e <sup>-7</sup>	100	TL159, TL255

Table 3: List of SO<sub>2</sub> assimilation experiments used in this paper. The main experiments discussed in Section 4 are the baseline experiment (BLexp) and the layer height experiment (LHexp). The additional experiments are used in the sensitivity studies in Section 4.2. Bg-error denotes background error, stdv standard deviation and hcor horizontal correlation length scale.

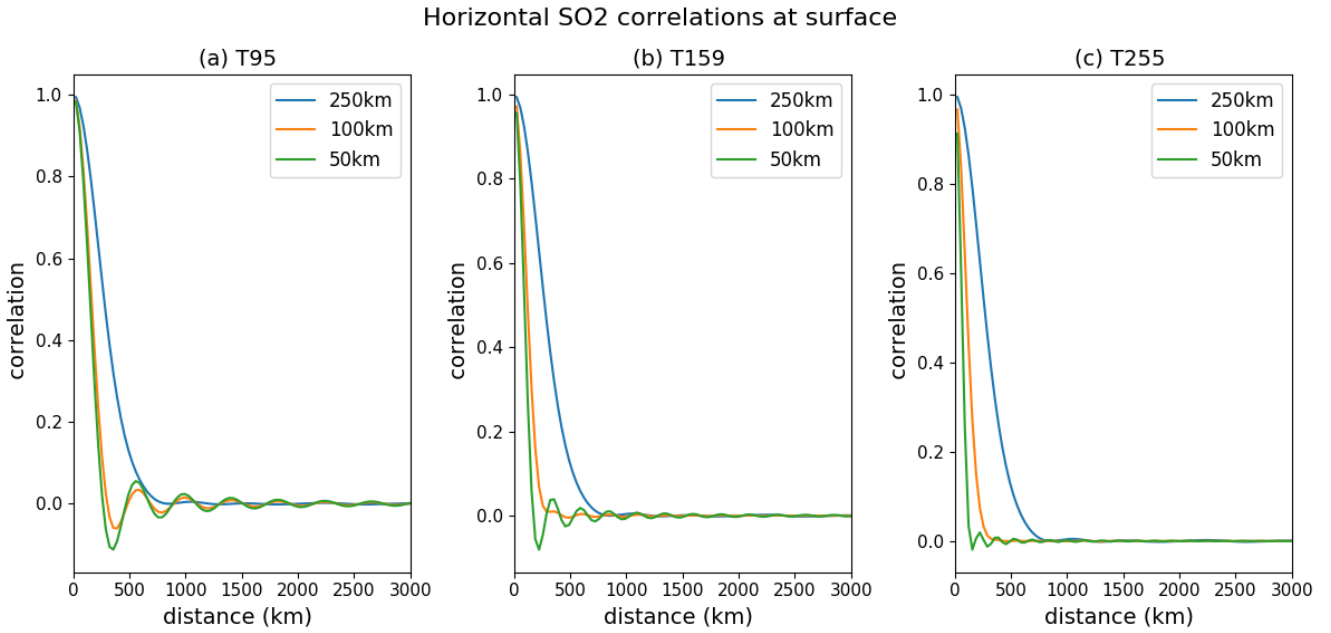
which assimilated NRT TROPOMI TCSO<sub>2</sub> data with the operational CAMS configuration and the layer height experiment (LHexp) which uses the FP\_ILM S5P LH data with a horizontal background error correlation length of 100 km and background error standard deviation values of 0.7e<sup>-7</sup> kg/kg are the main experiments used in this paper (Section 4.3 below) to assess if the assimilation of the SO<sub>2</sub> LH data using a more realistic height rather than the default 5 km improves the CAMS SO<sub>2</sub> analyses and forecasts. The other LH experiments assess the impact of using different horizontal SO<sub>2</sub> background error correlation length scales and various SO<sub>2</sub> background error standard deviation values. In all these experiments GOME-2 SO<sub>2</sub> data were not assimilated, and GOME-2B is used as a fully independent dataset for the validation.

The low resolution of the minimisation (TL95/TL159 in the CAMS system operational in 2021) is a factor that limits the ability of the SO<sub>2</sub> analysis to reproduce small-scale SO<sub>2</sub> features seen in the observations because it gives a lower limit for the length scale of the horizontal background error correlations that can be used, i.e. for the operational CAMS configuration only wavenumbers up to 95/159 can be represented. The smallest wavelength ( $\lambda_{min}$ ) that can be represented by two grid points on a linear grid is

$$\lambda_{min} = \frac{2\pi R}{n_{max}} \quad (1)$$

where R is the radius of the Earth and n<sub>max</sub> the maximum wavenumber of the truncation (95 or 159 for the inner loops in the operational CAMS configuration), i.e. twice the size of a grid box. This means that the minimum wavelengths which can be represented with two grid points for TL95, TL159 and TL255 are about 420 km, 250 km, 160 km, respectively and smaller scale horizontal structures cannot be represented in the background error wavelet formulation. Figure 4 illustrates this and shows horizontal SO<sub>2</sub> correlations at the surface for horizontal background error length scales of 50km, 100km and 250 km for truncations of TL95, TL159 and TL255. The ‘wriggles’ seen in the TL95 (and to a lesser extent in the TL159) plots show that the shorter background error correlations length scales cannot be properly resolved at these truncations. Even at TL255 some minor oscillations are still visible for horizontal correlation length scales of 50 km. Therefore, to properly resolve

smaller-scale plumes the resolutions of the inner loops would need to be even higher than TL255. Figure 4 also illustrates how far an increment from a single SO<sub>2</sub> observation would be spread out in the horizontal and therefore affect grid points away from the observation.



390

**Figure 4: SO<sub>2</sub> background error horizontal surface correlations at different truncations: (a) TL95, (b) TL159 and (c) TL255 if the horizontal length scales are specified as Gaussian correlation function with length scales of 250 km (blue), 100 km (orange) and 50 km (green).**

395 The operational NRT CAMS configuration uses minimisations at TL95/TL159 and a length scale of 250 km for the horizontal SO<sub>2</sub> background error correlations. For the data assimilation experiments shown in this paper we use inner loops of TL159/TL255 to allow us to use a Gaussian correlation function with a length scale of 100 km and therefore resolve slightly smaller-scale features than in the operational NRT CAMS system. The computational cost of one analysis cycle increases by about 20-30% when the spectral resolution of the minimisation is increased in this way, with the largest increase  
400 coming from the second minimisation which is about 50% computationally more expensive than at lower resolution. Figure 5 shows the CAMS TCSO<sub>2</sub> analysis fields on 27 June 2019 resulting from the assimilation of the TROPOMI SO<sub>2</sub> LH data when horizontal background error correlation length scales of 50, 100 and 250 km were used (experiments LH50, LH100, LH250), while using the same background error standard deviation profile of  $10^{-7}$  kg/kg in all cases. Also shown are the NRT TROPOMI and GOME-2B TCSO<sub>2</sub> data for that day. The figure illustrates the large impact of the horizontal background error correlation length scale on the SO<sub>2</sub> analysis, as the SO<sub>2</sub> plume is considerably more spread out in the CAMS analysis when longer horizontal correlations are used, and that better agreement with the features seen in the observations is found for shorter horizontal correlations. Figure 6 shows timeseries of SO<sub>2</sub> burden and plume area for a threshold of 5 DU from TROPOMI, GOME-2B and the three SO<sub>2</sub> LH experiments to further assess the impact on the SO<sub>2</sub> analysis of changing the horizontal correlation  
405

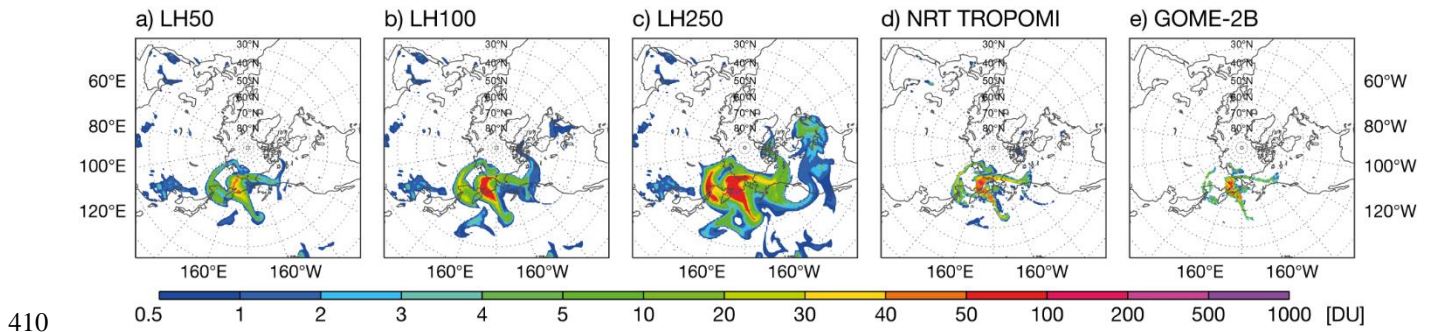


Figure 5: TCSO<sub>2</sub> analyses on 27 June 2019 at 0z obtained by assimilating SO<sub>2</sub> LH data using a background standard deviation profile of  $10^{-7}$  kg/kg and background errors with horizontal correlations of (a) 50 km, (b) 100 km and (c) 250 km. Also shown are (d) NRT TROPOMI and (e) GOME-2B TCSO<sub>2</sub> values.

length scale. We see that the SO<sub>2</sub> burden and plume area calculated from the observations are overestimated by all three CAMS TCSO<sub>2</sub> analyses. This overestimation is a well-known feature usually seen in the operational NRT CAMS volcanic SO<sub>2</sub> assimilation. Figure 6 illustrates that a major factor causing this overestimation is the choice of the horizontal background error correlation length scale and that by choosing a length scale of 250 km the SO<sub>2</sub> burden and plume area are about 6 times larger than for a length scale of 50 km. This implies that a limiting factor for correctly reproducing the SO<sub>2</sub> burden and plume area in the CAMS analysis is the resolution of the inner loops as it limits the horizontal correlation length scale that can be chosen for the background errors. A coarser inner loop resolution requires a longer horizontal length scale because shorter wavelengths cannot be resolved properly. If the aim is to reproduce finer-scale volcanic plumes with the CAMS data assimilation system, the horizontal resolution of the inner loops will have to be increased. For the main LH experiment used in this paper we decided to use a horizontal correlation length scale of 100 km which can be represented properly if the resolutions of the inner loops are TL159/TL255.

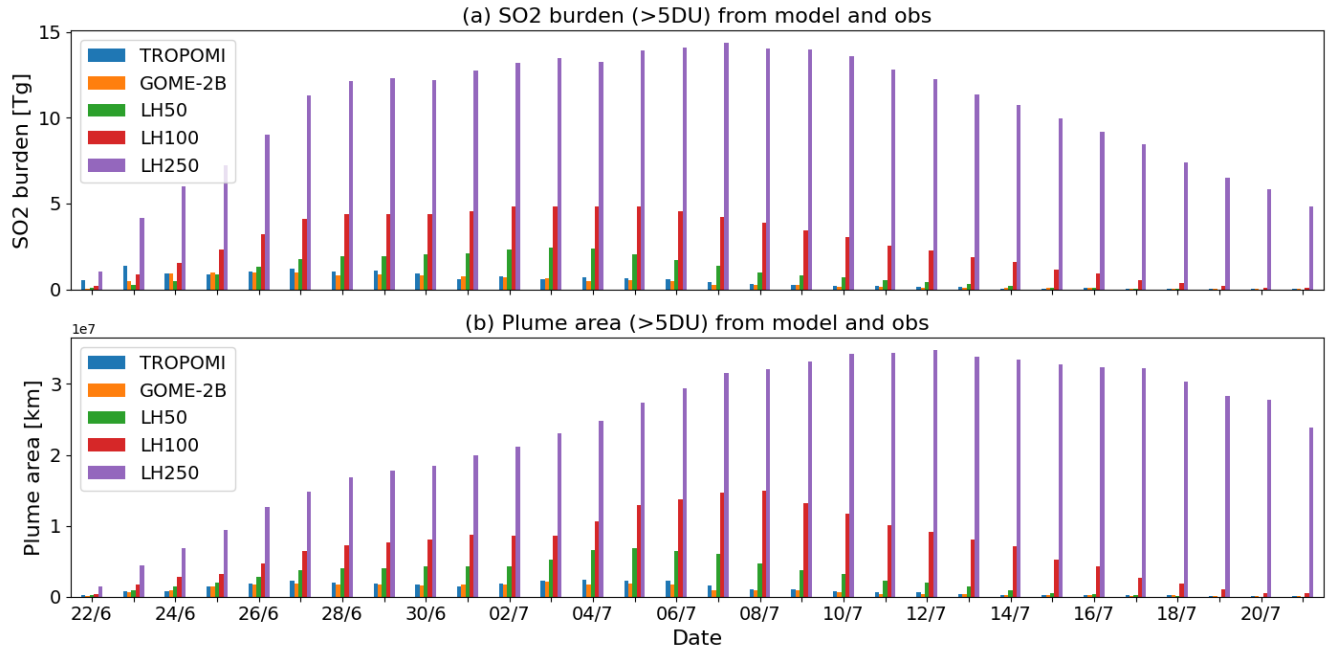
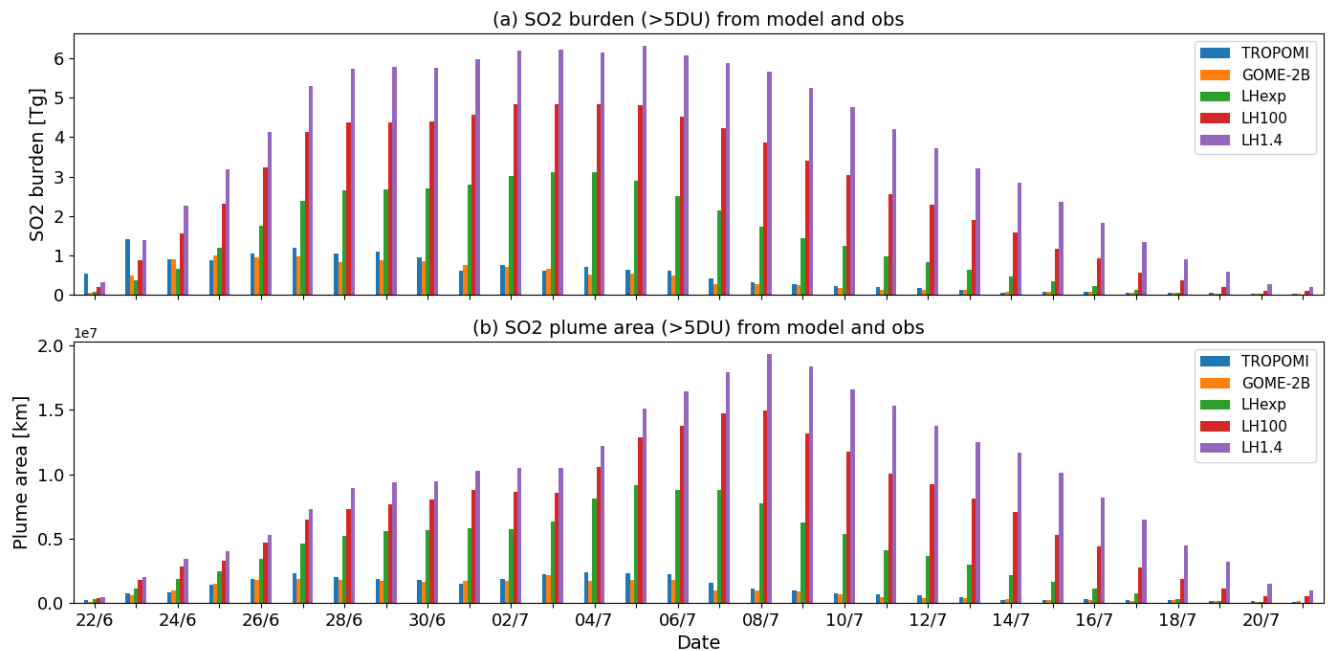


Figure 6: (a) SO<sub>2</sub> burden in Tg and (b) plume area in  $10^7$  km<sup>2</sup> from TROPOMI, GOME-2B and three SO<sub>2</sub> LH experiments at 0z with horizontal background error length scales of 50 km (LH50), 100km (LH100) and 250 km (LH250) for the Raikoke eruption (22 June to 21 July 2019). The values are calculated by gridding the data on a  $1^\circ \times 1^\circ$  grid and selecting the grid cells with TCSO<sub>2</sub> values greater than 5 DU in the area 30-90°N.

430

Another factor that influences the results of the SO<sub>2</sub> analysis is the value of the background error standard deviation profile. This is illustrated in Figure 7 which shows time series of SO<sub>2</sub> burden and plume area from TROPOMI, GOME-2B and three SO<sub>2</sub> LH experiments with varying background error standard deviation values ( $0.7 \times 10^{-7}$ ,  $1.0 \times 10^{-7}$ ,  $1.4 \times 10^{-7}$  kg/kg). All experiments used a horizontal background error correlation length scale of 100 km. The larger the background error standard deviation,

435 the larger the correction that is made by the SO<sub>2</sub> analysis and the larger the SO<sub>2</sub> burden and plume area become. However, the impact of changing the background error standard deviation is not as big as changing the horizontal background error correlation length scale and increasing the standard deviation value from 0.7e<sup>-7</sup> kg/kg to 1.4e<sup>-7</sup> kg/kg doubles the SO<sub>2</sub> burden and plume area.



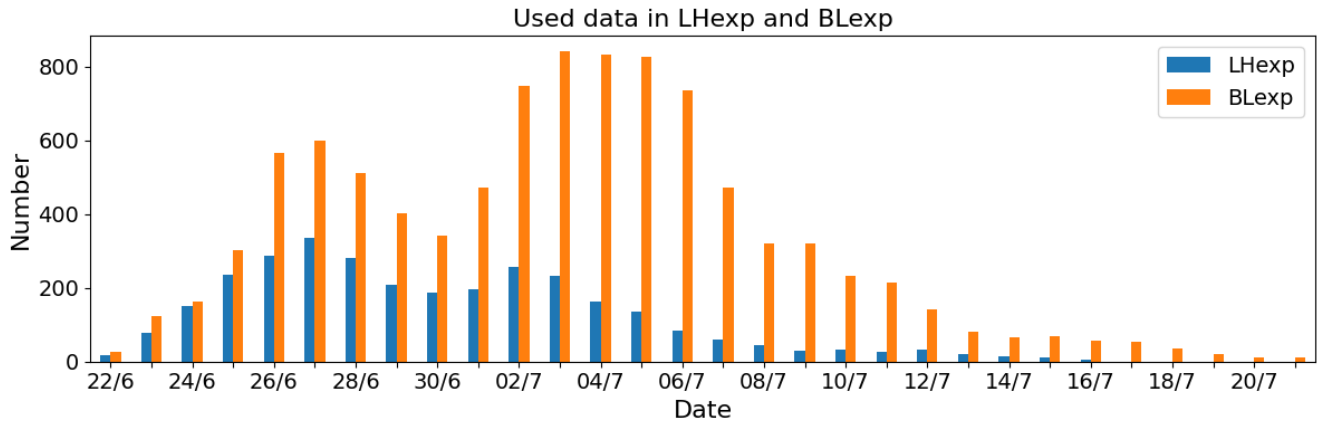
440 **Figure 7: (a) SO<sub>2</sub> burden in Tg and (b) plume area in 1e<sup>7</sup> km<sup>2</sup> from TROPOMI, GOME-2B and three SO<sub>2</sub> LH experiments at 0z with background error standard deviation values of 0.7e<sup>-7</sup> (LHexp), 1e<sup>-7</sup> (LH100) and 1.4e<sup>-7</sup> kg/kg (LH1.4) for the Raikoke eruption (22 June to 21 July 2019). The values are calculated by gridding the data on a 1°x1° grid and selecting the grid cells with TCSO<sub>2</sub> values greater than 5 DU in the area 30-90°N.**

445 For the remainder of this paper the LH experiment that uses a value of 0.7e-7 kg/kg for the background error standard deviation and a horizontal background error correlation length scale of 100 km is used (abbreviated as LHexp).

#### 4.3 Results of TCSO<sub>2</sub> assimilation tests for the Raikoke 2019 eruption

The SO<sub>2</sub> analysis fields and 5-day forecasts for the Raikoke eruption from the SO<sub>2</sub> layer height experiment (LHexp) and the baseline experiment with the CAMS configuration (BLexp) are now assessed in more detail. This assessment includes (1) a 450 visual inspection of the SO<sub>2</sub> analysis, (2) the assessment of the vertical location of the analysis SO<sub>2</sub> plume by comparison with independent IASI/ MetOp plume height observations and (3) the assessment of the quality of the 5-day SO<sub>2</sub> forecasts that are started from the LHexp and BLexp SO<sub>2</sub> analyses.

We evaluate the SO<sub>2</sub> analyses and forecasts against GOME-2B and TROPOMI NRT TCSO<sub>2</sub> data. GOME-2B TCSO<sub>2</sub> data 455 are fully independent because they are not used in our SO<sub>2</sub> assimilation experiments, and TROPOMI NRT TCSO<sub>2</sub> products are useful to demonstrate in how far the analyses manage to reproduce the TROPOMI TCSO<sub>2</sub> values. It has to be kept in mind that the version of the SO<sub>2</sub> LH product used in this study (v3.1) attains its optimal accuracy of 2km for SO<sub>2</sub> columns greater than 20 DU and hence, in LHexp, no TCSO<sub>2</sub> observations below 20 DU are assimilated. For the evaluation, the SO<sub>2</sub> analyses and forecasts, as well as the satellite data, are gridded onto a 1°x1° grid. Figure 8 shows a timeseries of the number 460 of observations that are actively assimilated in both experiments, i.e. the number of 1°x1° grid points with active observations, and illustrates that there are more active data in BLexp where NRT TROPOMI SO<sub>2</sub> data with values greater than 5 DU are assimilated (i.e. as done in the operational CAMS system) than in LHexp where only data with LH TCSO<sub>2</sub> greater than 20 DU are assimilated.



465 **Figure 8: Timeseries of number of active TROPOMI SO<sub>2</sub> observations assimilated in LHexp (blue) and BLexp (orange) both gridded on a 1°x1° grid (22 June to 21 July 2019).**

#### 4.3.1 Evaluation of TCSO<sub>2</sub> analyses

Figure 9 shows TCSO<sub>2</sub> maps from LHexp and BLexp as well as maps of TCSO<sub>2</sub> from NRT TROPOMI, GOME-2B and 470 FP\_ILM TROPOMI SO<sub>2</sub>LH data for 4 days: 22, 25, 29 June and 4 July 2019. The maps on 22 June capture the beginning of the eruption and show that the TCSO<sub>2</sub> values from the first analysis cycle in both experiments are lower than the observations. It also illustrates that even at this initial time the extent of the SO<sub>2</sub> plume is overestimated in both experiments. By 25 and 29 June the SO<sub>2</sub> plume already covers a big part of the North Pacific and by 4 July SO<sub>2</sub> from the eruption is detected in half the northern hemisphere. LHexp captures the structures of the SO<sub>2</sub> plumes seen in the observations better 475 than BLexp, but overall, both experiments capture the horizontal extent of the plume reasonably well. Figure 9 also illustrates that GOME-2B and NRT TROPOMI TCSO<sub>2</sub> show the same features of the plume, however the TROPOMI NRT lower detection limit facilitates the retrieval of smaller TCSO<sub>2</sub> values around the edges of the plumes. The FP\_ILM SO<sub>2</sub>LH product (v3.1) does not provide reliable information for TCSO<sub>2</sub> < 20 DU and therefore only picks up those parts of the plume that are associated with the highest SO<sub>2</sub> load. This also explains the lower number of active observations seen in 480 Fig.8. Especially during the later stages of the eruption parts of the plume are missed by the SO<sub>2</sub> LH product. Nevertheless, when assimilating the FP\_ILM SO<sub>2</sub> LH data we find good agreement with the NRT TROPOMI data and the GOME-2B data in LHexp (Fig. 9, column 1) when the CAMS analysis reports SO<sub>2</sub> values < 20DU.

Figure 10 shows timeseries of the SO<sub>2</sub> burden from NRT TROPOMI, GOME-2B and the two experiments calculated for 485 threshold values of 5 DU and 30 DU, and Figure 11 shows the corresponding timeseries of the plume areas. For the lower

threshold of 5 DU both the SO<sub>2</sub> burden and the plume area are overestimated in LHexp and BLexp. This confirms what was

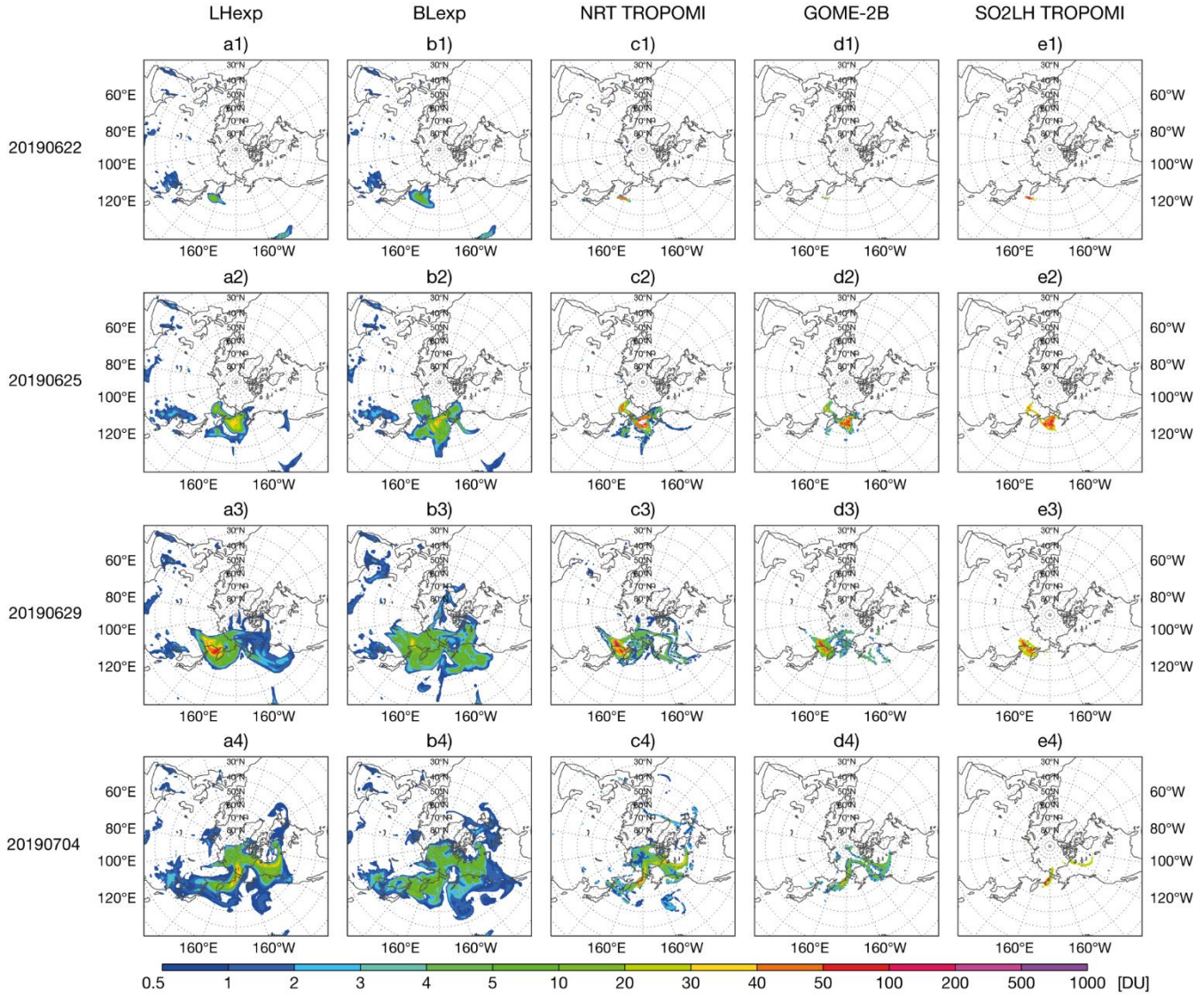


**Figure 9: TCSO<sub>2</sub> analysis fields at 0z from LH exp (a), BL experiment (b), NRT TROPOI (c), NRT GOME-2B (d) and TROPOMI SO<sub>2</sub>LH (e) on 22 June (row 1), 25 June (row 2), 29 June (row 3) and 4 July (row 4) in DU. In panels (c)-(e) all available observations are shown, illustrating that the SO<sub>2</sub> LH product only picks up those parts of the plume that are associated with the highest SO<sub>2</sub> load.**

490

already seen in Figures 6 to 8, namely that the plumes are more spatially dispersed in the analysis than in the observations. The overestimation of the SO<sub>2</sub> burden is larger in LHexp than in BLexp with maximum values of 3 Tg and 2 Tg, 495 respectively, compared to 1.5 and 1.2 Tg for NRT TROPOMI and GOME-2B. However, the plume area is larger in BLexp with maximum extent of about 1e<sup>7</sup> km<sup>2</sup>, compared to 0.8e<sup>7</sup> km<sup>2</sup> in LHexp and 0.2e<sup>7</sup>km<sup>2</sup> calculated from the observations. The larger overestimation of the SO<sub>2</sub> burden in LHexp is the result of differences in the background error standard deviation values used in the experiments and of the fact that lower SO<sub>2</sub> columns, which could correct an overestimation in parts of the plume, are not assimilated. BLexp fails to capture the higher SO<sub>2</sub> column values, leading to an underestimation of plume 500 area and SO<sub>2</sub> burden for a threshold of 30 DU, while LHexp does have TCSO<sub>2</sub> values > 30 DU but overestimates both plume area and SO<sub>2</sub> burden.

To quantify the realism of the SO<sub>2</sub> analyses and the quality of the SO<sub>2</sub> forecasts appropriate error measures need to be defined and used in addition to the visual inspection of the SO<sub>2</sub> plumes. Statistical measures such as bias and root mean 505 square error are not well suited because of the specific event character of the SO<sub>2</sub> plumes. In addition to looking at the plume

area and SO<sub>2</sub> burden, we use threshold-based measures based on the number of hits (grid boxes where both model and observations detect the plume), misses (grid boxes where there is a plume in the observations but not in the model) or false alarms (grid boxes where the model has volcanic SO<sub>2</sub> that is not seen in the observations) to quantify the error in the plume position. In Flemming and Inness (2013) we used hits and plume area measures for various thresholds. In this paper we 510 combine the information about hits and misses and use as score the probability of detection (POD)

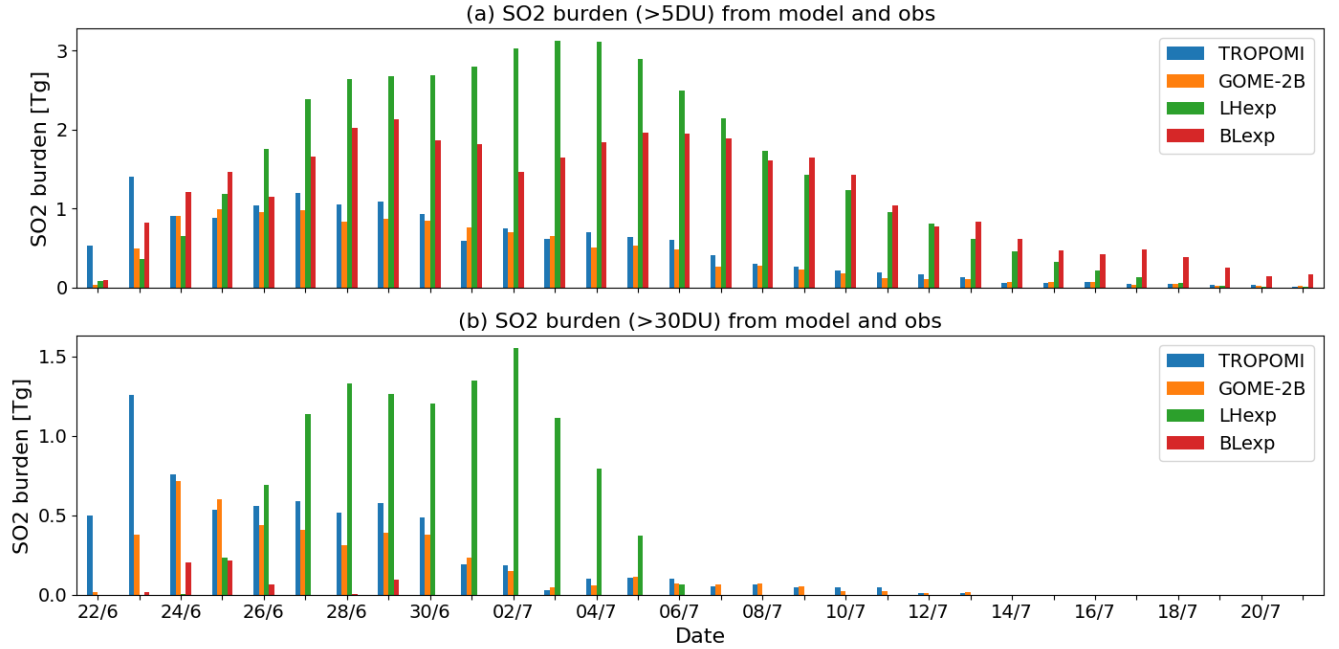


Figure 10: SO<sub>2</sub> burden in Tg from TROPOMI, GOME-2B, LHexp and BLexp TCSO<sub>2</sub> analysis at 0z for the Raikoke eruption (22 June to 21 July 2019). The values are calculated by gridding the data on a 1°x1° grid and selecting the grid cells with TCSO<sub>2</sub> values greater than (a) 5 DU and (b) 30 DU in the area 30-90°N.

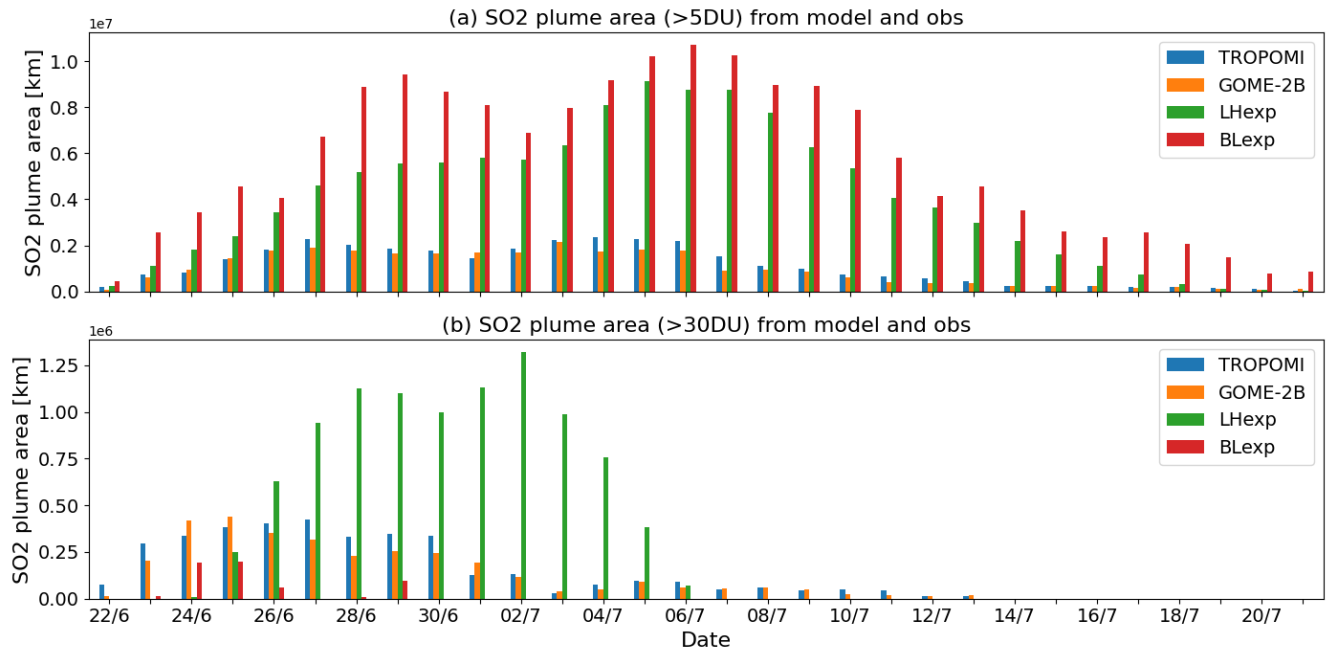


Figure 11: SO<sub>2</sub> plume area [km<sup>2</sup>] from TROPOMI, GOME-2B, LHexp and BLexp TCSO<sub>2</sub> analysis at 0z for the Raikoke eruption (22 June to 21 July 2019). The values are calculated by gridding the data on a 1°x1° grid and selecting the grid cells with TCSO<sub>2</sub> values greater than (a) 5 DU and (b) 30 DU in the area 30-90°N.

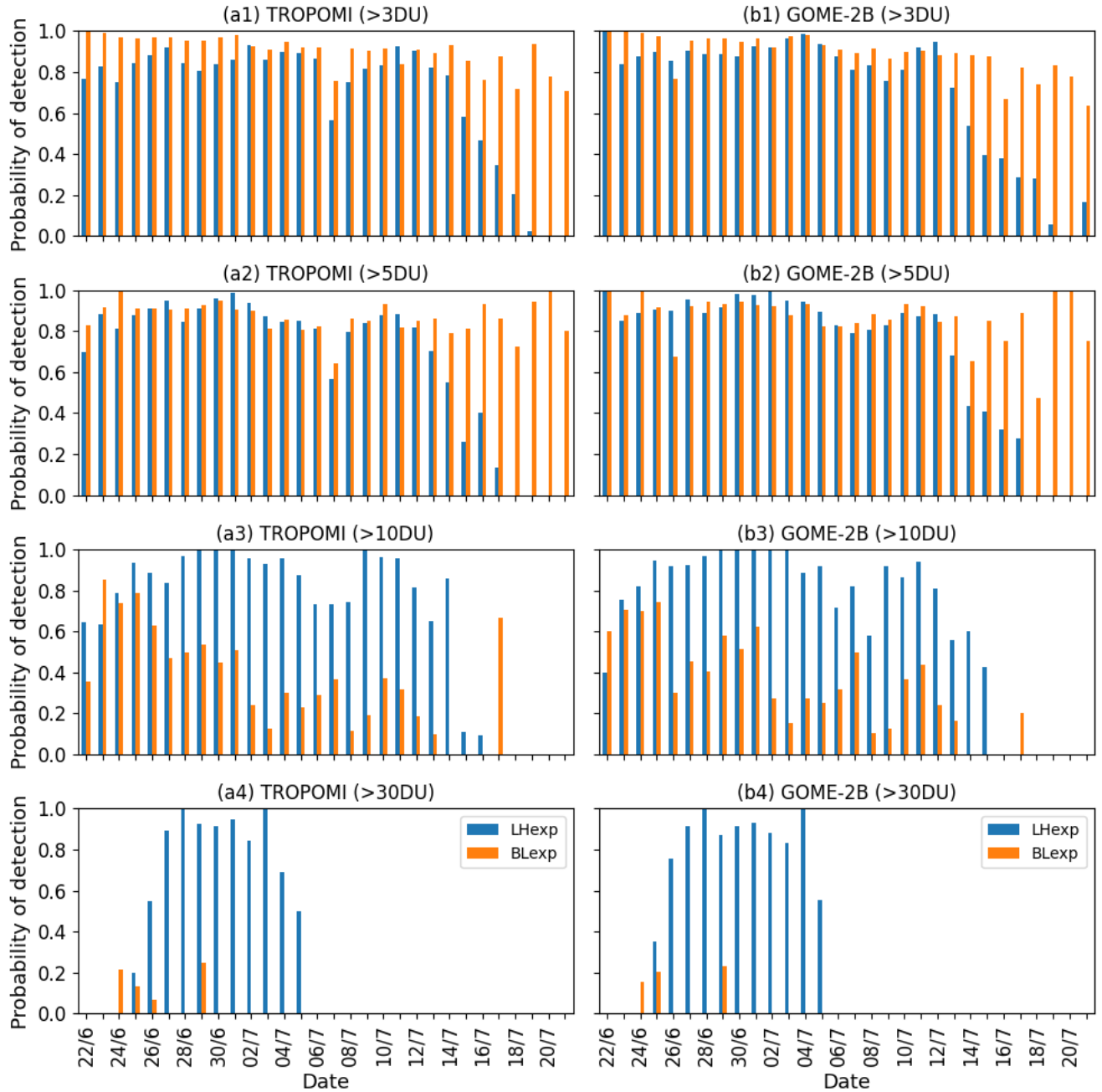
520

$$POD = \text{hits} / (\text{hits} + \text{misses}) \quad (2)$$

which lies between 0 and 1, with a value of 1 indicating a perfect score. We also use the critical success index (CSI), defined as

$$\text{CSI} = \text{hits}/(\text{hits} + \text{misses} + \text{false alarms}) \quad (3)$$

525 which additionally considers the number of false alarms and again has values between 0 and 1 with 1 indicating a perfect score (Nurmi, 2003). These are point based comparisons and might score badly for features that are close but slightly misplaced between observations and model.



530 **Figure 12:** Timeseries of POD for TCSO<sub>2</sub> analysis fields (at 0z) against (a) NRT TROPOMI and (b) GOME-2B for TCSO<sub>2</sub> thresholds of (1) 3DU, (2) 5 DU, (3) 10 DU and (4) 30 DU (22 June to 21 July 2019). Values for LHexp are shown in blue, values for BLexp in orange.

535 Figure 12 shows the POD from LHexp and BLexp for various TCSO<sub>2</sub> analysis thresholds (3, 5, 10, 30 DU) scored against NRT TROPOMI and GOME-2B data. The results are very similar for both satellites. The parts of the plume with lower TCSO<sub>2</sub> values are well captured by both experiments with POD values above 0.9 for BLexp for most of the period and POD

values above 0.8 for LHexp. The POD in LHexp decreases towards the end of the depicted period because the number of assimilated data drops strongly (see Fig. 8), while more observations are assimilated in BLexp at the later stage of the episode. BLexp, however, does not capture the higher values observed by NRT TROPOMI and GOME-2B well while LHexp has a much higher POD for those parts of the plume. No values above 30 DU are detected after 5 July 2019.

Figure 13 shows the CSI from LHexp and BLexp, the measure that also penalises the false alarms. As expected, these values are considerably lower than the POD (with maximum values around 0.6) because plume area and  $\text{SO}_2$  burden are overestimated in both experiments (see Fig. 9) leading to numerous false alarms. Both experiments behave similarly for the lower thresholds but TCSO<sub>2</sub> values greater than 30 DU are again captured better in LHexp.

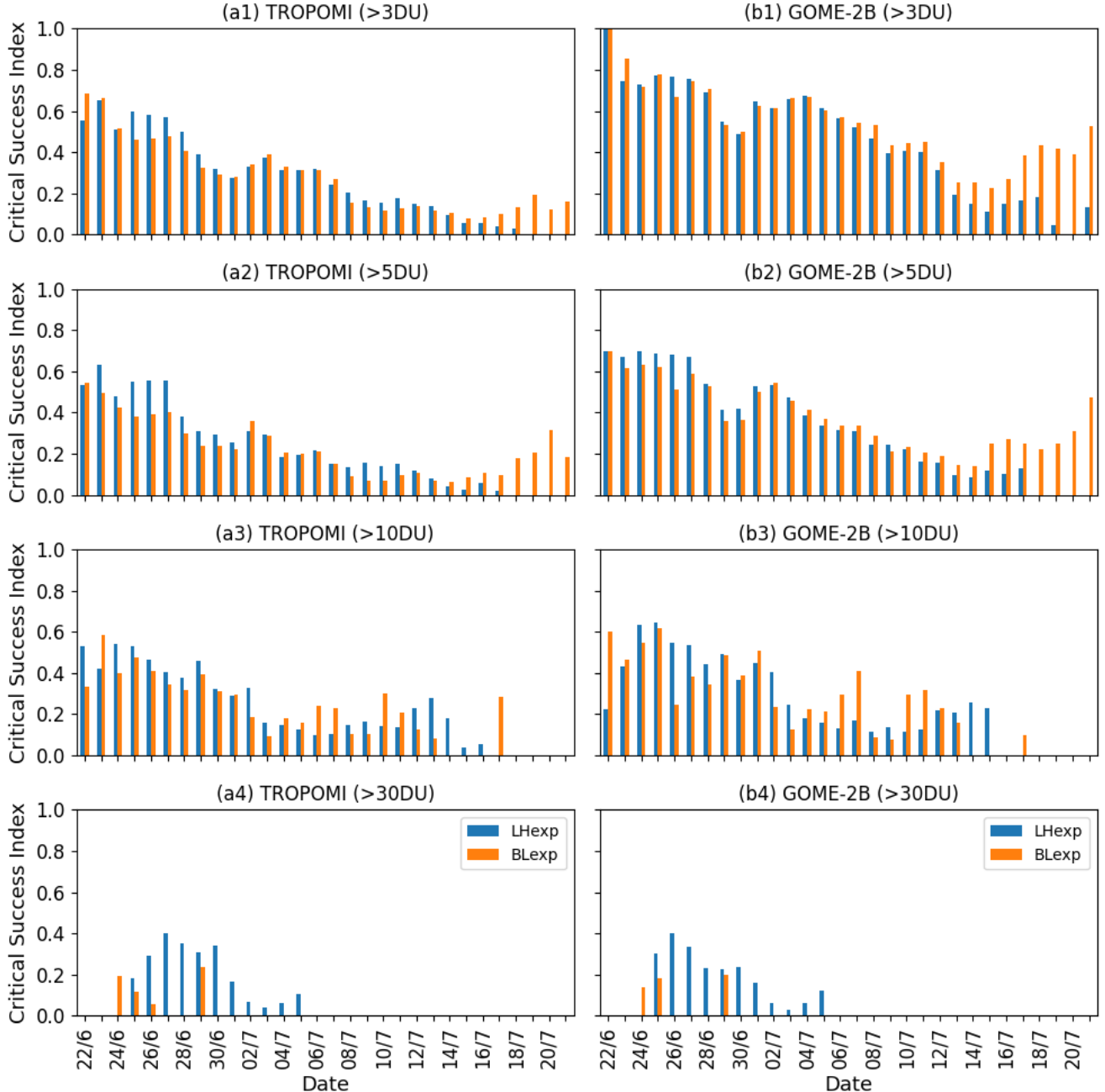


**Figure 13: Timeseries of CSI for TCSO<sub>2</sub> analysis fields (at 0z) against (a) NRT TROPOMI and (b) GOME-2B for TCSO<sub>2</sub> thresholds of (1) 3DU, (2) 5 DU, (3) 10 DU and (4) 30 DU (22 June to 21 July 2019). Values for LHexp are shown in blue, values for BLexp in orange.**

In summary, as far as the TCSO<sub>2</sub> analysis fields are concerned the performance of LHexp and BLexp is similar for TCSO<sub>2</sub> columns below 10 DU, but BLexp does not capture the higher SO<sub>2</sub> values as well as LHexp. Both experiments overestimate the SO<sub>2</sub> burden and the plume area compared to the TROPOMI NRT and GOME-2B observations.

### 555 4.3.2 Vertical location of the SO<sub>2</sub> plume

While the TCSO<sub>2</sub> analyses from LHexp and BLexp score similarly in the detection of the TCSO<sub>2</sub> plume observations by GOME-2B and NRT TROPOMI, at least for values less than 10 DU, the vertical distributions of the SO<sub>2</sub> plumes from the experiments differ considerably. Figure 14 shows vertical cross sections along 60°N between 120-300°E through the SO<sub>2</sub> plume on 29 June 2019 from LHexp and BLexp. The figure illustrates that the bulk of the SO<sub>2</sub> plume is located between 560 200-100 hPa in LHexp while it is located much lower, between 600-400 hPa, in BLexp. To assess which vertical distribution is more realistic, in Figure 15 we compare the plume heights from the experiments with SO<sub>2</sub> altitudes derived from IASI LATMOS ULB data (Clarisso et al., 2012) for the period 22 to 29 June 2019. The CAMS plume altitude was calculated as the altitude where the highest SO<sub>2</sub> value were found in the CAMS SO<sub>2</sub> profiles. The figure shows that the plume height in LHexp agrees well with the independent IASI plume altitude with a mean bias of 0.4±2.2 km, while BLexp underestimates the plume altitude with a mean bias of -5.1±2.1 km. Figure 15 illustrates that the altitude of the Raikoke SO<sub>2</sub> plume in the 565 CAMS analysis is considerably improved if SO<sub>2</sub>LH data are used than when using the baseline configuration.

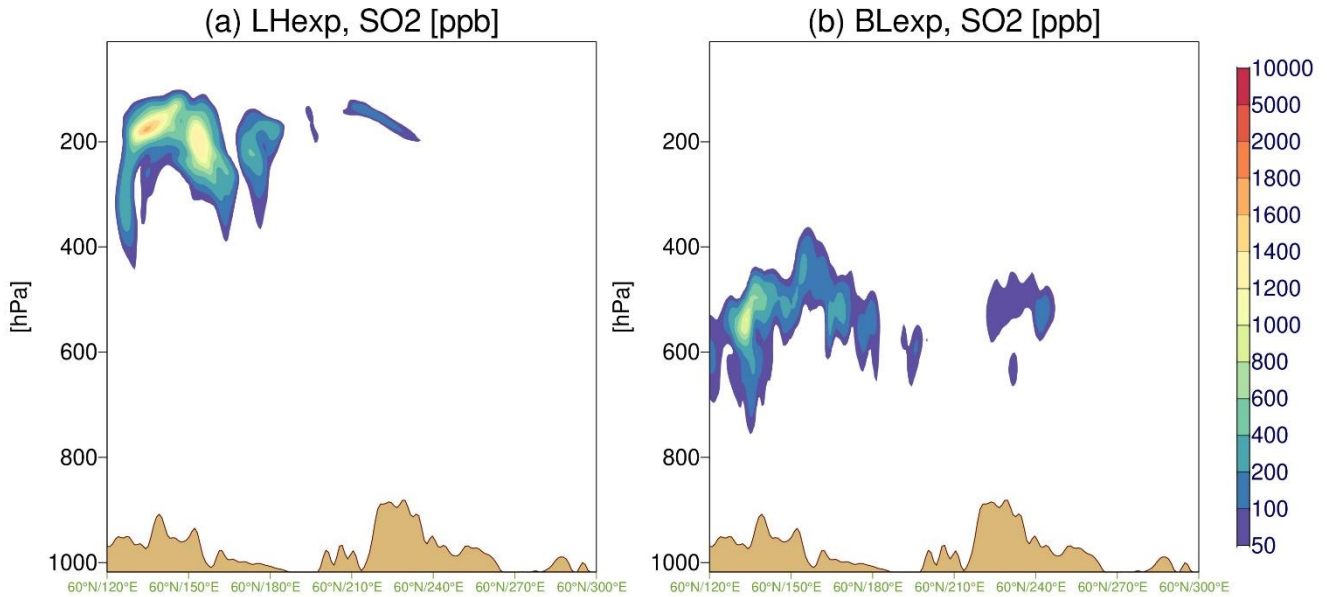
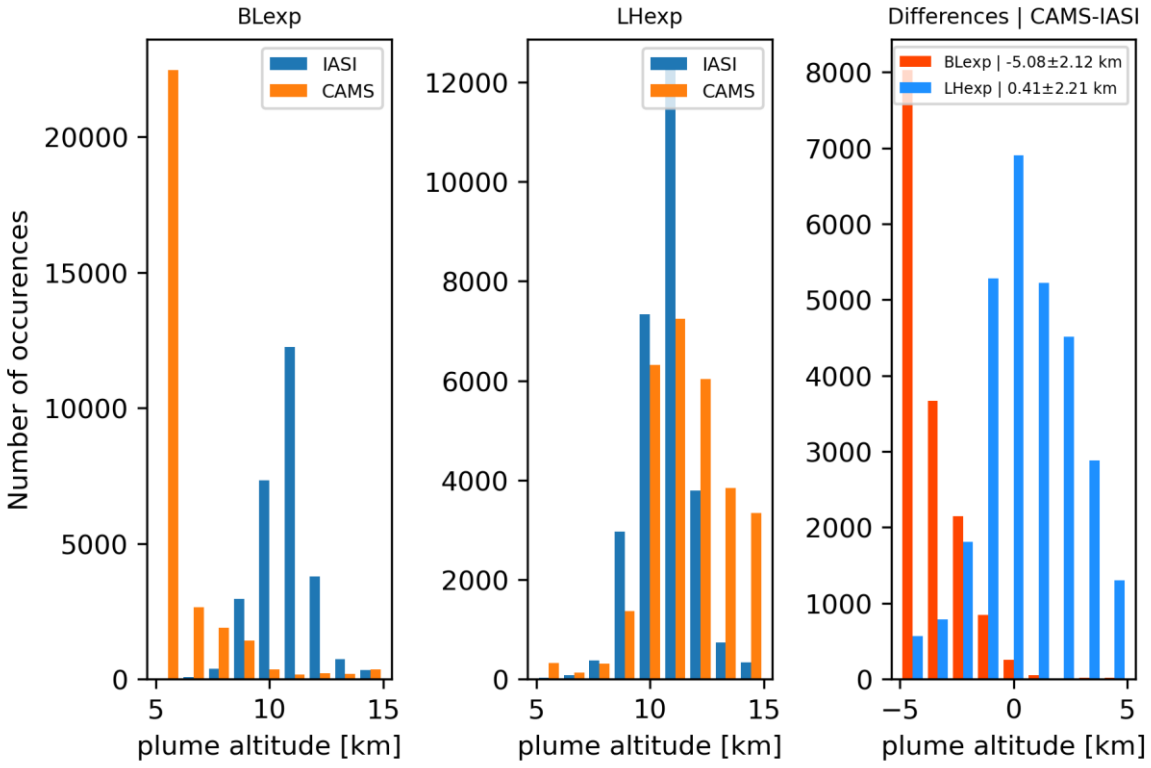


Figure 14: Vertical cross sections along 60°N between 120-300°E showing the SO<sub>2</sub> analysis field (in ppb) from (a) LHexp and (b) BLexp on 29 June 2019, 0z.



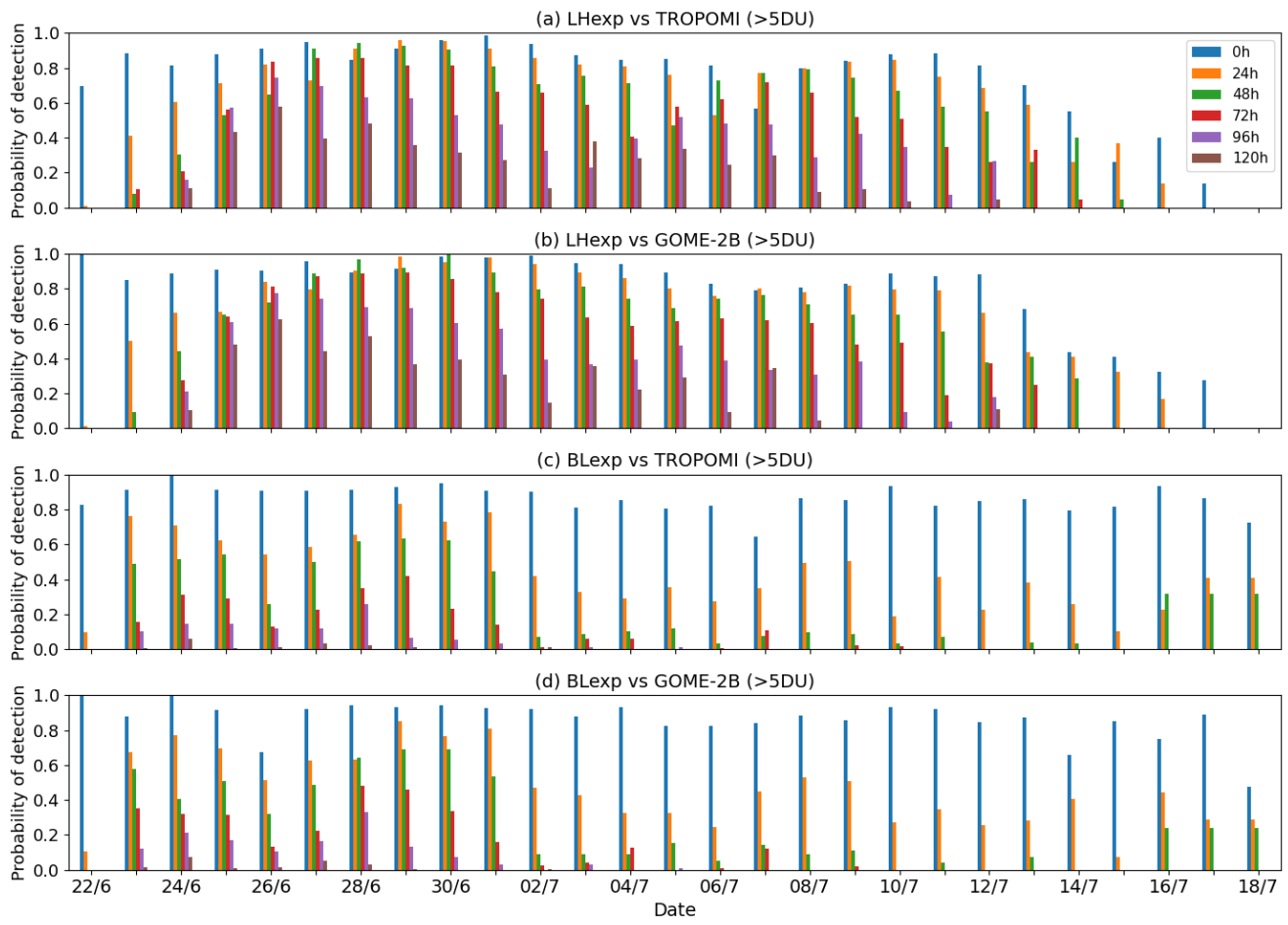
570

**Figure 15: Comparison of plume altitude from IASI ULB LATMOS data with the altitude of maximum  $\text{SO}_2$  concentration from the LHexp (middle panel) and BLExp (left panel) for the period 22-29 June 2019. The right panel shows a histogram of the differences of the plume altitudes (CAMS minus IASI) for LHexp (blue) and BLExp (red).**

575

#### 4.3.3 Quality of the 5-day TCSO<sub>2</sub> forecasts

Next, we assess the quality of the 5-day TCSO<sub>2</sub> forecasts started from the LHexp and BLExp SO<sub>2</sub> analyses. Figure 16 shows a timeseries of POD for a TCSO<sub>2</sub> threshold of 5 DU from LHexp and BLExp for NRT TROPOMI and GOME-2B for the initial SO<sub>2</sub> analysis and forecasts valid on the same day at different lead-times (24 to 120 hours). The figure shows that the skill decreases with increasing forecast lead-time in both experiments, but that the degradation of skill with forecast lead-time is considerably large in BLExp. For the 72-hour forecasts LHexp has POD values between 0.6 and 0.8 and even the 96-hour forecast still has values of 0.4. In contrast, BLExp only has POD values between 0.2 and 0.4 for the 72-hour forecasts



585 **Figure 16: Probability of detection of LHexp against (a) NRT TROPOMI and (b) GOME-2B, as well as BLexp against (c) NRT TROPOMI and (d) GOME-2B for the period 22 June to 18 July 2021 for analysis at 0z (blue), 24-hour forecast (orange), 48-hour forecast (green), 72-hour forecast (red), 96-hour forecast (purple) and 120-hour forecast (brown).**

590 during June while values drop considerably during July when even the short 24-hour forecasts from BLexp only have POD values between 0.2 and 0.4. In other words, in BLexp the skill of forecasting the location of the SO<sub>2</sub> plumes seen by GOME-  
2B and the NRT TROPOMI one day in advance is similar to the skill of forecasting the SO<sub>2</sub> plumes 4 days in advance in  
LHexp. The main reason for the lower forecast quality in BLexp is the fact that the SO<sub>2</sub> plumes are located at the wrong  
altitude (see Fig. 15) so that the prevailing winds will not transport the SO<sub>2</sub> in the correct direction.

600 To further assess the forecast skill, we use the fractional skill score (FSS) which is a spatial comparison. It was originally used to assess the quality of precipitation forecasts (Roberts and Lean, 2007) but has more recently also been used to assess the skill of dispersion models to capture volcanic plumes (de Leeuw et al., 2021; Dacre et al., 2016; Harvey and Dacre, 2016). The FSS is calculated using the ratio of the modelled and observed fractional coverage of the SO<sub>2</sub> plume at each location for various horizontal scales (neighbourhoods) and thresholds, and it assesses how the skill of the forecast varies depending on those parameters. To calculate it we grid the model TCSO<sub>2</sub> analyses and forecasts at various lead-times and the NRT TROPOMI and GOME-2B TCSO<sub>2</sub> observations on a 1°x1° grid and create binary fields for the chosen thresholds (in our case for TCSO<sub>2</sub> > 1, 3, 5, 10, 20, 30, 50 DU). Then, for each grid point, the fraction of surrounding grid points that exceed the threshold is calculated from the model field and the observations. To establish at which horizontal scale the SO<sub>2</sub> analysis or forecast is useful we repeat this exercise with neighbourhoods of varying scales (i.e. 1, 3, 5°, corresponding to neighbourhoods of 1, 9 and 25 grid boxes, respectively). An FSS of 1 means perfect alignment of the features in the observations and the model and an FSS of 0 a total mismatch. We use values of FSS greater than 0.5 to define a simulation that has some skill. This value was also used by de Leeuw et al. (2021) and Harvey and Dacre (2016). The FSS for a neighbourhood of length n is calculated following Roberts and Lean (2007) as

$$FSS_{(n)} = 1 - \frac{MSE_{(n)}}{MSE_{(n)ref}} \quad (4)$$

where MSE is the Mean Square Error and  $MSE_{(n)}=0$  for a perfect forecast of neighbourhood with length n. The reference

610 MSE for each neighbourhood length n is given by:

$$MSE_{(n)ref} = \frac{1}{N_x N_y} \left[ \sum_{i=1}^{N_x} \sum_{j=1}^{N_y} O_{(n)i,j}^2 + \sum_{i=1}^{N_x} \sum_{j=1}^{N_y} M_{(n)i,j}^2 \right] \quad (5)$$

Here  $i=1, N_x$  with  $N_x$  the number of columns in the domain and  $j=1, N_y$  with  $N_y$  the number of rows.  $M_{(n)i,j}$  is the field of model fractions obtained from the model binary field for a square of length n and  $O_{(n)i,j}$  the corresponding field of observed fractions.  $MSE_{(n)ref}$  can be interpreted as the largest possible MSE that can be obtained from the model and observed fractions.

615

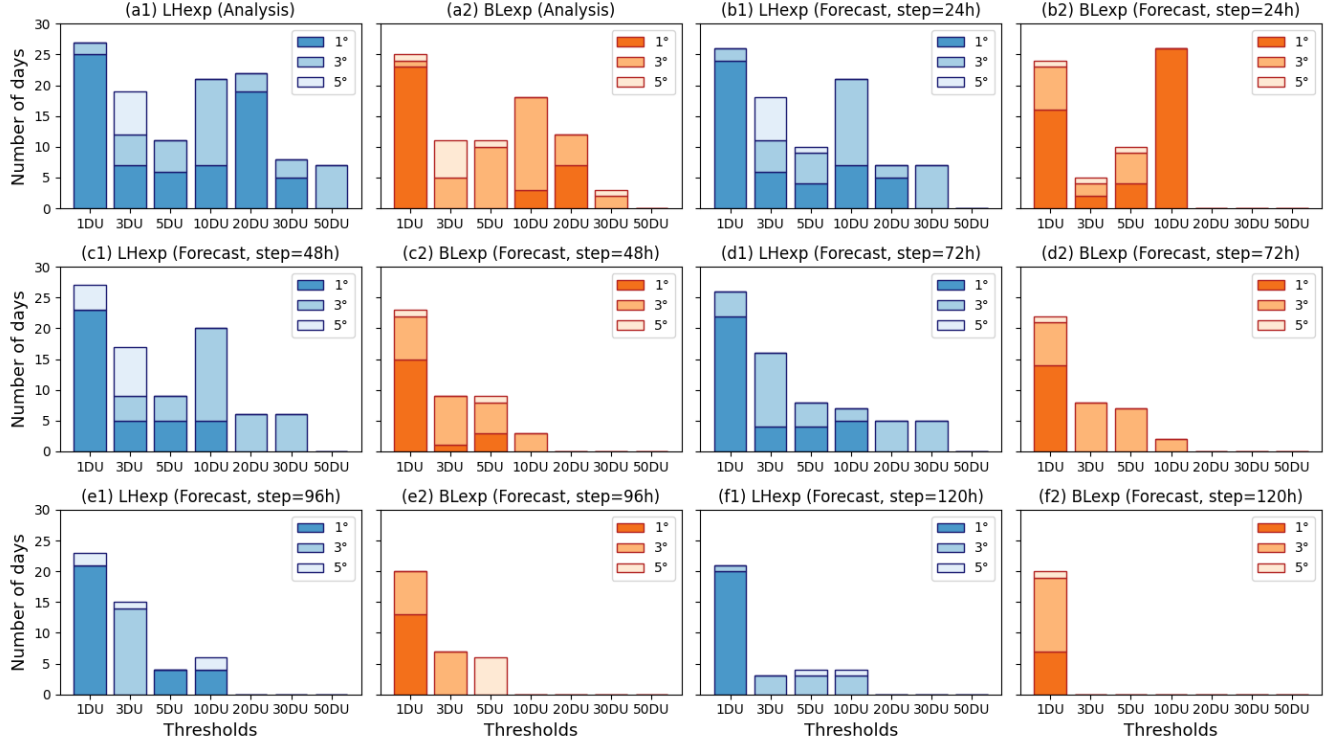


**Figure 17: Number of days since the eruption on 22 June 2019 that the LHexp (blue) and BLexp (orange) (a) analyses and forecasts at steps (b) 24, (c) 48, (d) 72, (e) 96 and (f) 120-hours have some skill ( $FSS > 0.5$ ) compared to NRT TROPOMI TCSO<sub>2</sub> data for neighbourhood sizes of 1°, 3° and 5° and thresholds of 1, 3, 5, 10, 20, 30, 50 DU.**

620 Figure 17 shows the number of days after the eruption that have  $FSS > 0.5$  when comparing LHexp and BLexp with NRT TROPOMI data for the various thresholds, to give some indication of a skill timescale, i.e. how long the analyses and the forecasts started from them can be considered as useful after the initial eruption. Also shown (in the lighter shadings) are the additional useful forecast days that are gained when the neighbourhood size is increased to 3° or 5°. The main findings of the figure are (1) the skill timescale is longer for the smaller thresholds, i.e. the overall shape of the plume is easier to reproduce 625 than smaller scale filaments with higher TCSO<sub>2</sub> values, (2) the skill timescale drops with lead-time, (3) the skill timescale increases if the neighbourhood size is increased, with a larger increase for higher thresholds, pointing to errors in the location of structures with higher TCSO<sub>2</sub>, which are reduced with a larger grid, and (4) that the skill timescale is greater in LHexp than in BLexp, leading to better forecasts of the plume longer in advance, as already seen in Fig. 16.

630 We now look at the individual panels in more detail. Figure 17a shows the skill timescales of the TCSO<sub>2</sub> analyses from LHexp and BLexp against NRT TROPOMI and illustrates as already seen in Section 4.3.1 that these give similarly useful TCSO<sub>2</sub> fields (especially for the lower thresholds), but that the number of useful days is slightly larger in LHexp and that BLexp fails to capture the highest TCSO<sub>2</sub> values. It is interesting to see the large number of days with  $FSS > 0.5$  for the

threshold of 20 DU in LHexp, because this is the value below which no TCSO<sub>2</sub> data are assimilated in LHexp. Figure 17b  
635 shows that the 24-hour forecasts in LHexp have similar skill to the analysis, which a skill timescale of 24 days for the 1 DU  
threshold and a neighbourhood size of 1°, illustrating that the 24-hour from the LHexp analysis can predict the overall  
location of the SO<sub>2</sub> plume very well. For higher thresholds (> 30 DU) this drops to about 5 days after the eruption, and there  
640 is no skill for a threshold of 50 DU. The skill of the 48 and 72-hour forecasts (Fig. 17c and d) are similar to that of the 24-  
hour one for the thresholds up to 10 DU, but at a neighbourhood size of 1° the higher values (>20 DU) have no skill  
645 anymore. As there is still skill on a 5-day timescale for these forecasts for a neighbourhood size of 3°, this suggests that it is  
the location of the filaments with high TCSO<sub>2</sub> values that is not correct rather than the forecast not maintaining any of the  
higher TCSO<sub>2</sub> values. Even the 96 and 120-hour forecasts (Fig. 17e and f) in LHexp have a skill timescale of slightly more  
650 than 20 days for the 1 DU threshold at 1°, but the skill drops markedly for the higher thresholds, and for the 120-hour  
forecasts skill is only found for thresholds up to 10 DU at 3° for up to 3 days after the eruption. Nevertheless, Fig. 17 shows  
655 that by assimilating SO<sub>2</sub> LH data the CAMS system can predict the overall location of the SO<sub>2</sub> plume up to 5 days in  
advance for about 20 days after the initial eruption. This corresponds to the time when the SO<sub>2</sub> LH product does not detect  
volcanic SO<sub>2</sub> anymore (see Fig. 8). Leeuw et al. (2021), using the Met Office's Numerical Atmospheric-dispersion  
Modelling Environment (NAME) dispersion model, found skill timescales of 12–17 days for low density (> 1 DU) parts of  
the Raikoke SO<sub>2</sub> cloud and shorter skill timescales of 2–4 days for the denser parts of the cloud (> 20 DU). It is interesting  
660 to see skill timescales of similar magnitude to the ones obtained in our study even though their method is different. Leeuw et  
al. (2021) initialized the NAME dispersion model with eruption source parameters and then followed the evolution of the  
SO<sub>2</sub> cloud, while we use data assimilation to update the location of the plume daily and provide daily forecasts with a  
maximum length of 5 days.

655 Figure 17 shows that the BLexp analysis has skill timescales similar to LHexp, confirming what was already seen in Figures  
12 and 13. Despite placing the SO<sub>2</sub> cloud at the wrong altitude, the overall shape of the SO<sub>2</sub> plume is still captured by the  
SO<sub>2</sub> analysis. However, for higher thresholds the number of useful days after the eruption is smaller in BLexp and the  
forecast skill drops more steeply with forecast lead-time than in LHexp. There is no skill for the 24-hour forecast at 1° for  
660 thresholds greater than 20 DU, and for the 48-hour forecasts the skill timescale for a 1 DU threshold at 1° is 15 days,  
compared to 23 days in LHexp. The skill timescale remains around 14 days in BLexp for the 72 and 96-hour forecasts for a 1  
DU threshold at 1° and then drops to 6 days at 120-hours. For the 72 to 120-hour forecasts there is no skill for the higher  
thresholds for a neighbourhood size of 1°, pointing to a worse misplacement of the smaller scale features of the plume with  
higher TCSO<sub>2</sub> values than in LHexp.

665 For GOME-2B (not shown) the number of useful forecast days are generally slightly lower, especially for a threshold of 1  
DU which might just be an artefact because GOME-2B does not detect so many volcanic pixels with low values. For  
thresholds of 3–30 DU the GOME-2 results for a neighbourhood size of 1° or 3° are very similar to the TROPOMI results for  
all the forecast ranges, with skill timescales of about 10 days for forecast lead times up to 72 hour and around 5 days for the  
96-hour forecasts. Again, the performance of BLexp is worse than of LHexp and for the 48-hour forecasts there is almost no  
670 skill in BLexp for the 1° neighbourhoods.

## 5 Conclusions

In this paper we document the procedure used to assimilate near-real time TCSO<sub>2</sub> data from the TROPOMI and GOME-2  
instruments in the operational CAMS NRT data assimilation system and explore the use of TROPOMI SO<sub>2</sub> layer height data  
provided by the ESA-funded Sentinel-5P Innovation–SO<sub>2</sub> Layer Height Project and produced with the Full-Physics Inverse

675 Learning Machine algorithm (v3.1) developed by DLR. The assimilation of the FP\_ILM SO<sub>2</sub> LH data was tested for the 2019 Raikoke eruption and compared with results obtained when assimilating NRT TROPOMI TCSO<sub>2</sub> data with the operational CAMS configuration.

680 While the operational CAMS approach of placing the SO<sub>2</sub> increment in the mid-troposphere around 550 hPa gives surprisingly good results for the TCSO<sub>2</sub> analyses and short-range forecasts in a lot of situation (including this case), the vertical distribution of SO<sub>2</sub> in the baseline analysis is clearly wrong for the Raikoke eruption which injected a copious amount of SO<sub>2</sub> into the stratosphere. By using the FP\_ILM TROPOMI SO<sub>2</sub> LH data this can be much improved as comparison with the independent SO<sub>2</sub> plume heights retrieved from IASI show. While the LH experiment agrees well with the IASI LATMOS ULB plume altitude products, with a mean bias of 0.4±2.2 km, the baseline experiment underestimates 685 the plume altitude with a mean bias of -5.1±2.1 km. Consequently, the assimilation of the FP\_JLM LH data leads to much improved SO<sub>2</sub> forecasts and should improve the usefulness of the CAMS SO<sub>2</sub> forecasts for users and also for the aviation industry.

690 In the baseline experiment the forecast skill drops much more for longer forecast lead-times than in the LH experiment, which is seen when comparing point skill scores such as probability of detection and critical success index and when using the fractional skill score that also assesses spatial skill. Timeseries of the Probability of Detection score show that in the baseline experiment, the skill of forecasting the location of the Raikoke SO<sub>2</sub> plume seen by GOME-2B and the NRT TROPOMI one day in advance is similar to the skill of forecasting the SO<sub>2</sub> plume 4 days in advance in LHexp. The FSS shows that compared to NRT TROPOMI, even the 120-hour forecasts of the LH experiment have a significant skill up to 20 695 days after the initial eruption for the prediction of TCSO<sub>2</sub> for a 1 DU threshold and a neighbourhood size of 1°, suggesting that the overall location of the SO<sub>2</sub> plume is well reproduced. The skill is smaller for higher TCSO<sub>2</sub> thresholds (about 5 days for forecast ranges up to 96-hours on a 1° grid), illustrating that it is more difficult to accurately predict the location of areas with higher SO<sub>2</sub> columns which usually have smaller spatial scales. The skill timescale is shorter for the baseline experiment, with values around 15 days after the initial eruption for the 1 DU threshold for forecast ranges up to 96-hours and 5 days for 700 the 120-hours forecasts, but there is no skill for any of the higher thresholds at a neighbourhood size of 1° from 72-hour forecasts onwards. By assimilating FP\_ILM SO<sub>2</sub> LH data the CAMS system can predict the overall location of the Raikoke SO<sub>2</sub> plume up to 5 days in advance for about 20 days after the initial eruption.

705 Our study also documents some issues of the CAMS TCSO<sub>2</sub> assimilation approach, namely the overestimation of the SO<sub>2</sub> burden and plume area by the data assimilation system, both in the operational configuration and when using the FP\_ILM SO<sub>2</sub> LH data. The main reason for this overestimation is the coarse horizontal resolution used in the minimisations (currently TL95 and TL159 in the operational CAMS system) which limits the wavenumbers that can be resolved in the wavelet formulation of the SO<sub>2</sub> background errors. This in turn limits the horizontal correlation length scale that can be used for the SO<sub>2</sub> background errors and that determines how for the increments from individual observations are spread out in the 710 horizontal. In this paper we used TL159/TL255 as the resolutions for the minimisations, but to properly resolve small scale structures the resolutions of the minimisations would have to be even higher. Obviously, this would increase the numerical cost of running the minimisation.

715 Other reasons that can contribute to an overestimation of the SO<sub>2</sub> burden or plume area in the CAMS SO<sub>2</sub> analysis could be the use of anthropogenic SO<sub>2</sub> emissions in the CAMS model as the satellite data used for the comparisons are only the volcanic pixels. However, tests run without the anthropogenic emissions (not shown in this paper) did not show large differences compared to the experiments presented here, suggesting that this is not a big effect for the Raikoke eruption.

Another possibility could be the fact that the satellite might miss a plume or part of a plume, but that the whole plume is present in the model. Finally, for the FP\_ILM LH product the data are limited to  $\text{TCSO}_2 > 20 \text{ DU}$  (in v3.1) and lower values 720 that might correct an overestimation from the previous analysis cycle are not used. In future we hope to also test the assimilation of IASI  $\text{SO}_2$  data with plume height information that would add extra information in the CAMS system.

One limitation in using the TROPOMI  $\text{SO}_2$  LH data is that the version used in this study (v3.1) only produces reliable 725 information for  $\text{TCSO}_2 > 20 \text{ DU}$  so that most of the smaller volcanic eruptions that happen on a more regular basis than big explosive eruptions would be missed if only the FP\_ILM TROPOMI  $\text{SO}_2$  LH data were assimilated in the CAMS NRT system. Improvements to the TROPOMI  $\text{SO}_2$  LH product are on-going so that it should be possible to lower this limit in the future.

## Code and Data availability

This study was based on the IFS model cycle 47R1. The ECWMF IFS code is only available subject to a licence agreement 730 with ECMWF. ECMWF member-state weather services and their approved partners will get access granted. The IFS code without modules for assimilation can be obtained for educational and academic purposes as part of the openIFS release (<https://confluence.ecmwf.int/display/OIFS>, last access 26/10/2021). A software licensing agreement with ECMWF is required to access the OpenIFS source distribution: despite the name it is not provided under any form of open-source 735 software license. License agreements are free, limited to non-commercial use, forbid any real-time forecasting, and must be signed by research or educational organizations. Personal licenses are not provided. OpenIFS can-not be used to produce or disseminate real-time forecast products. ECMWF has limited resources to provide support and thus may temporarily cease issuing new licenses if it is deemed too difficult to provide a satisfactory level of support. Provision of an OpenIFS software 740 license does not include access to ECMWF computers or data archives other than public datasets. A detailed documentation of the IFS code is available from <https://www.ecmwf.int/en/publications/ifs-documentation> (last access 26/10/2021). The output from the assimilation experiments used in this study is available from <https://apps.ecmwf.int/research-experiments/expver/> (last access 26/10/2021) using the following DOIs for the 6 experiments:

- hhu5: 10.21957/cygt-xf49
- hgze: 10.21957/qfam-7474
- hhbu: 10.21957/zpdt-f079
- hhtm: 10.21957/jraa-s174
- hhtn: 10.21957/ddxs-2v95
- hgz7: 10.21957/81bh-7h58

The TROPOMI V3.1  $\text{SO}_2$  LH data are available from <https://doi.org/10.5281/zenodo.5602935>, the operational TROPOMI  $\text{SO}_2$  data from the Copernicus Open Access Hub (<https://scihub.copernicus.eu/>) and the IASI  $\text{SO}_2$  plume height data from 750 <https://en.aeris-data.fr/>.

## Acknowledgements

The Copernicus Atmosphere Monitoring Service is operated by the European Centre for Medium-Range Weather Forecasts on behalf of the European Commission as part of the Copernicus program (<http://copernicus.eu>) and CAMS data are freely available from [atmosphere.copernicus.eu/data](http://atmosphere.copernicus.eu/data). The  $\text{SO}_2$  analysis and forecast experiments used in this paper are available 755 from <https://apps.ecmwf.int/research-experiments/expver/> (see DOIs in Table 3). The FP\_ILM TROPOMI  $\text{SO}_2$  LH product was developed in the framework of the ESA Sentinel-5p Innovation project. MEK would like to acknowledge the Aristotle

University of Thessaloniki (AUTH) High Performance Computing Infrastructure and Resources and the help of the AUTH IT Center. MEK further acknowledges the use of the Atmospheric Toolbox®. IASI is a joint mission of EUMETSAT and the Centre National d'Etudes Spatiales (CNES, France). The authors acknowledge the AERIS data infrastructure, 760 <https://en.aeris-data.fr/>, for providing access to the IASI SO<sub>2</sub> plume height data used in this study and ULB-LATMOS for the development of the retrieval algorithms. Thanks to Anabel Bowen for improving Figures 5 and 9.

## Author Contributions

AI prepared the code to assimilate the SO<sub>2</sub> LH data, ran the analysis experiments, carried out most of the validation and wrote the paper. MA helped with the construction of the background error matrices. JF provided help with the modelling 765 framework and RR wrote the converter software to transfer the SO<sub>2</sub> LH data from their native netcdf format to the BUFR format used in the ECMWF data assimilation system. MEK and DB performed the validation against the IASI/MetOp SO<sub>2</sub> plume altitude data and provided Fig. 15. PH provided the SO<sub>2</sub> LH data and developed the FP\_ILM algorithm. DE and DL also contributed to the FP\_ILM developments. All co-authors provided useful feedback on the paper.

## References

770 Albert, M. F. M. A., Anguelova, M. D., Manders, A. M. M., Schaap, M., and de Leeuw, G.: Parameterization of oceanic whitecap fraction based on satellite observations, *Atmos. Chem. Phys.*, 16, 13725–13751, <https://doi.org/10.5194/acp-16-13725-2016>, 2016.

Brenot, H., Theys, N., Clarisse, L., van Geffen, J., van Gent, J., Van Roozendael, M., van der A, R., Hurtmans, D., Coheur, 775 P.-F., Clerbaux, C., Valks, P., Hedelt, P., Prata, F., Rasson, O., Sievers, K., and Zehner, C.: Support to Aviation Control Service (SACS): an online service for near-real-time satellite monitoring of volcanic plumes, *Nat. Hazards Earth Syst. Sci.*, 14, 1099-1123, doi:10.5194/nhess-14-1099-2014, 2014.

Brenot, H., Theys, N., Clarisse, L., van Gent, J., Hurtmans, D. R., Vandenbussche, S., Papagiannopoulos, N., Mona, L., 780 Virtanen, T., Uppstu, A., Sofiev, M., Bugliaro, L., Vázquez-Navarro, M., Hedelt, P., Parks, M. M., Barsotti, S., Coltelli, M., Moreland, W., Arnold-Arias, D., Hirtl, M., Peltonen, T., Lahtinen, J., Sievers, K., Lipok, F., Rüfenacht, R., Haefele, A., Hervo, M., Wagenaar, S., Som de Cerff, W., de Laat, J., Apituley, A., Stammes, P., Laffineur, Q., Delcloo, A., Lennart, R., Rokitansky, C.-H., Vargas, A., Kerschbaum, M., Resch, C., Zopp, R., Plu, M., Peuch, V.-H., Van Roozendael, M., and Wotawa, G.: EUNADICS early warning system dedicated to support aviation in case of crisis from natural airborne hazard 785 and radionuclide cloud, *Nat. Hazards Earth Syst. Sci. Discuss.* [preprint], <https://doi.org/10.5194/nhess-2021-105>, in review, 2021.

Carn, S.A., Clarisse, L. and Prata, A.J.: Multi-decadal Satellite Measurements of Global Volcanic Degassing. *Journal of Volcanology and Geothermal Research*, 311, 99-134. doi:10.1016/j.jvolgeores.2016.01.002, 2016.

790

Clarisse, L., Hurtmans, D., Clerbaux, C., Hadji-Lazaro, J., Ngadi, Y., and Coheur, P.-F.: Retrieval of sulphur dioxide from the infrared atmospheric sounding interferometer (IASI), *Atmos. Meas. Tech.*, 5, 581–594, <https://doi.org/10.5194/amt-5-581-2012>, 2012.

795 Clarisse, L., Coheur, P.-F., Theys, N., Hurtmans, D., and Clerbaux, C.: The 2011 Nabro eruption, a SO<sub>2</sub> plume height analysis using IASI measurements, *Atmos. Chem. Phys.*, 14, 3095–3111, <https://doi.org/10.5194/acp-14-3095-2014>, 2014.

Clerbaux, C., Hadji-Lazaro, J., Turquety, S., et al., Tracking pollutants from space: Eight years of IASI satellite observation, Comptes Rendus Geoscience, Volume 347, Issue 3, Pages 134-144, <https://doi.org/10.1016/j.crte.2015.06.001>, 2015.

800

Courtier, P., Thépaut, J.-N., and Hollingsworth, A.: A strategy for operational implementation of 4D-Var, using an incremental approach, *Q. J. Roy. Meteor. Soc.*, 120, 1367–1388, 1994.

Dacre, H. F., et al. (2011), Evaluating the structure and magnitude of the ash plume during the initial phase of the 2010  
805 Eyjafjallajökull eruption using lidar observations and NAME simulations, *J. Geophys. Res.*, 116, D00U03,  
doi:10.1029/2011JD015608.

de Leeuw, J., Schmidt, A., Witham, C. S., Theys, N., Taylor, I. A., Grainger, R. G., Pope, R. J., Haywood, J., Osborne, M., and Kristiansen, N. I.: The 2019 Raikoke volcanic eruption – Part 1: Dispersion model simulations and satellite retrievals of  
810 volcanic sulfur dioxide, *Atmos. Chem. Phys.*, 21, 10851–10879, <https://doi.org/10.5194/acp-21-10851-2021>, 2021.

Diamantakis, M. and Flemming, J.: Global mass fixer algorithms for conservative tracer transport in the ECMWF model, *Geosci. Model Dev.*, 7, 965–979, doi:10.5194/gmd-7-965-2014, 2014

815 Efremenko, D. S., Loyola R., D. G., Hedelt, P., and Spurr, R. J. D.: Volcanic SO<sub>2</sub> plume height retrieval from UV sensors using a full-physics inverse learning machine algorithm, *Int. J. Remote Sens.*, 38, 1–27,  
<https://doi.org/10.1080/01431161.2017.1348644>, 2017.

820 Fedkin, N. M., Li, C., Krotkov, N. A., Hedelt, P., Loyola, D. G., Dickerson, R. R., and Spurr, R.: Volcanic SO<sub>2</sub> effective layer height retrieval for the Ozone Monitoring Instrument (OMI) using a machine-learning approach, *Atmos. Meas. Tech.*, 14, 3673–3691, <https://doi.org/10.5194/amt-14-3673-2021>, 2021.

825 Fisher, M. and Andersson, E.: Developments in 4D-Var and Kalman Filtering, ECMWF Technical Memorandum 347, available from ECMWF, Shinfield Park, Reading, Berkshire, RG2 9AX, UK, 2001,  
<https://www.ecmwf.int/sites/default/files/elibrary/2001/9409-developments-4d-var-and-kalman-filtering.pdf>

Fisher, M.: Generalized frames on the sphere with application to background error covariance modelling, Seminar on resent developments in numerical methods for atmospheric and ocean modelling, 6–10 September 2004, Proceedings, ECMWF, pp.87–101, available from ECMWF, Shinfield Park, Reading, Berkshire, RG2 9AX, UK, 2004.

830

Fisher, M.: Wavelet Jb – A new way to model the statistics of back-ground errors, ECMWF Newsletter, 106, 23–28, available from ECMWF, Shinfield Park, Reading, Berkshire, RG2 9AX, UK, 2006.

835 Flemming, J., and Inness, A. (2013), Volcanic sulfur dioxide plume forecasts based on UV satellite retrievals for the 2011 Grímsvötn and the 2010 Eyjafjallajökull eruption, *J. Geophys. Res. Atmos.*, 118, 10,172– 10,189, doi:10.1002/jgrd.50753.

Flemming, J., Huijnen, V., Arteta, J., Bechtold, P., Beljaars, A., Blechschmidt, A.-M., Diamantakis, M., Engelen, R. J., Gaudel, A., Inness, A., Jones, L., Josse, B., Katragkou, E., Marecal, V., Peuch, V.-H., Richter, A., Schultz, M. G., Stein, O.,

and Tsikerdekis, A.: Tropospheric chemistry in the Integrated Forecasting System of ECMWF, *Geosci. Model Dev.*, 8, 975–840 1003, <https://doi.org/10.5194/gmd-8-975-2015>, 2015.

Flemming, J., Benedetti, A., Inness, A., Engelen, R. J., Jones, L., Huijnen, V., Remy, S., Parrington, M., Suttie, M., Bozzo, A., Peuch, V.-H., Akritidis, D., and Katragkou, E.: The CAMS interim Reanalysis of Carbon Monoxide, Ozone and Aerosol for 2003–2015, *Atmos. Chem. Phys.*, 17, 1945–1983, <https://doi.org/10.5194/acp-17-1945-2017>, 2017

845

Goitom, B., Oppenheimer, C., Hammond, J. O. S., Grandin, R., Barnie, T., Donovan, A., Ogubazghi, G., Yohannes, E., Kibrom, G., Kendall, J.-M., et al.: First recorded eruption of Nabro volcano, Eritrea, 2011, *B. Volcanol.*, 77, 85, <https://doi.org/10.1007/s00445-015-0966-3>, 2015

850 Granier, C., S. Darras, H. Denier van der Gon, J. Doubalova, N. Elguindi, B. Galle, M. Gauss, M. Guevara, J.-P. Jalkanen, J. Kuenen, C. Liousse, B. Quack, D. Simpson, K. Sindelarova, The Copernicus Atmosphere Monitoring Service global and regional emissions (April 2019 version), Copernicus Atmosphere Monitoring Service (CAMS) report, 2019, doi:10.24380/d0bn-kx16.

855 Grebennikov, V.S., Zubachev, D.S., Korshunov, V.A. et al. Observations of Stratospheric Aerosol at Rosgidromet Lidar Stations after the Eruption of the Raikoke Volcano in June 2019. *Atmos. Ocean Opt.* 33, 519–523 (2020). <https://doi.org/10.1134/S1024856020050097>

860 Harvey, N. J. and Dacre, H. F.: Spatial evaluation of volcanic ash forecasts using satellite observations, *Atmos. Chem. Phys.*, 16, 861–872, <https://doi.org/10.5194/acp-16-861-2016>, 2016.

Hedelt, P., Efremenko, D. S., Loyola, D. G., Spurr, R., and Clarisse, L.: Sulfur dioxide layer height retrieval from Sentinel-5 Precursor/TROPOMI using FP\_ILM, *Atmos. Meas. Tech.*, 12, 5503–5517, <https://doi.org/10.5194/amt-12-5503-2019>, 2019.

865 Huijnen, V., Williams, J., van Weele, M., van Noije, T., Krol, M., Dentener, F., Segers, A., Houweling, S., Peters, W., de Laat, J., Boersma, F., Bergamaschi, P., van Velthoven, P., Le Sager, P., Eskes, H., Alkemade, F., Scheele, R., Nédélec, P., and Pätz, H.-W.: The global chemistry transport model TM5: description and evaluation of the tropospheric chemistry version 3.0, *Geosci. Model Dev.*, 3, 445–473, <https://doi.org/10.5194/gmd-3-445-2010>, 2010.

870 Huijnen, V., Pozzer, A., Arteta, J., Brasseur, G., Bouarar, I., Chabriat, S., Christophe, Y., Doumbia, T., Flemming, J., Guth, J., Josse, B., Karydis, V. A., Marécal, V., and Pelletier, S.: Quantifying uncertainties due to chemistry modelling – evaluation of tropospheric composition simulations in the CAMS model (cycle 43R1), *Geosci. Model Dev.*, 12, 1725–1752, <https://doi.org/10.5194/gmd-12-1725-2019>, 2019

875 Inness, A., Blechschmidt, A.-M., Bouarar, I., Chabriat, S., Crepulja, M., Engelen, R. J., Eskes, H., Flemming, J., Gaudel, A., Hendrick, F., Huijnen, V., Jones, L., Kapsomenakis, J., Katragkou, E., Keppens, A., Langerock, B., de Mazière, M., Melas, D., Parrington, M., Peuch, V. H., Razinger, M., Richter, A., Schultz, M. G., Suttie, M., Thouret, V., Vrekoussis, M., Wagner, A., and Zerefos, C.: Data assimilation of satellite-retrieved ozone, carbon monoxide and nitrogen dioxide with ECMWF's Composition-IFS, *Atmos. Chem. Phys.*, 15, 5275–5303, <https://doi.org/10.5194/acp-15-5275-2015>, 2015.

880 Inness, A., Ades, M., Agustí-Panareda, A., Barré, J., Benedictow, A., Blechschmidt, A.-M., Dominguez, J. J., Engelen, R., Eskes, H., Flemming, J., Huijnen, V., Jones, L., Kipling, Z., Massart, S., Parrington, M., Peuch, V.-H., Razinger, M., Remy,

S., Schulz, M., and Suttie, M.: The CAMS reanalysis of atmospheric composition, *Atmos. Chem. Phys.*, 19, 3515–3556, <https://doi.org/10.5194/acp-19-3515-2019>, 2019.

885 Koukouli, M.-E., Michailidis, K., Hedelt, P., Taylor, I. A., Inness, A., Clarisse, L., Balis, D., Efremenko, D., Loyola, D., Grainger, R. G., and Retscher, C.: Volcanic SO<sub>2</sub> Layer Height by TROPOMI/S5P; validation against IASI/MetOp and CALIOP/CALIPSO observations, *Atmos. Chem. Phys. Discuss.* [preprint], <https://doi.org/10.5194/acp-2021-936>, in review, 2021.

890 Laloyaux P., Bonavita M., Chrust M., Gürol S. Exploring the potential and limitations of weak-constraint 4D-Var. *Q J R Meteorol Soc.* 2020;146:4067–4082.. [org/10.1002/qj.3891](https://doi.org/10.1002/qj.3891)

Loyola, D. G., Xu, J., Heue, K.-P., and Zimmer, W.: Applying FP\_ILM to the retrieval of geometry-dependent effective Lambertian equivalent reflectivity (GE\_LER) daily maps from UVN satellite measurements, *Atmos. Meas. Tech.*, 13, 985–999, <https://doi.org/10.5194/amt-13-985-2020>, 2020.

895 Moxnes, E. D., Kristiansen, N. I., Stohl, A., Clarisse, L., Durant, A., Weber, K., and Vogel, A. (2014), Separation of ash and sulfur dioxide during the 2011 Grímsvötn eruption, *J. Geophys. Res. Atmos.*, 119, 7477–7501, doi:10.1002/2013JD021129.

900 Munro, R., Lang, R., Klaes, D., Poli, G., Retscher, C., Lindstrot, R., Huckle, R., Lacan, A., Grzegorski, M., Holdak, A., Kokhanovsky, A., Livschitz, J., and Eisinger, M.: The GOME-2 instrument on the Metop series of satellites: instrument design, calibration, and level 1 data processing – an overview, *Atmos. Meas. Tech.*, 9, 1279–1301, <https://doi.org/10.5194/amt-9-1279-2016>, 2016.

905 Muser, L. O., Hoshayripour, G. A., Bruckert, J., Horváth, Á., Malinina, E., Wallis, S., Prata, F. J., Rozanov, A., von Savigny, C., Vogel, H., and Vogel, B.: Particle aging and aerosol–radiation interaction affect volcanic plume dispersion: evidence from the Raikoke 2019 eruption, *Atmos. Chem. Phys.*, 20, 15015–15036, <https://doi.org/10.5194/acp-20-15015-2020>, 2020.

910 Nurmi (2003): Recommendations on the verification of local weather forecasts. ECMWF Technical Memorandum, no. 430, <https://www.ecmwf.int/node/11401>

Parrish, D. F. and Derber, J. C.: The National Meteorological Center's spectral statistical-interpolation analysis scheme, *Mon. Weather Rev.*, 120, 1747–1763, 1992.

915 Platt, U. and Stutz, J.: Differential Optical Absorption Spectroscopy (DOAS): Principle and Applications, Springer, Berlin, 2008

920 Platt, U. (2017). Air Monitoring by Differential Optical Absorption Spectroscopy. In *Encyclopedia of Analytical Chemistry*, R.A. Meyers (Ed.). <https://doi.org/10.1002/9780470027318.a0706.pub2>

Prata, F., Woodhouse, M., Huppert, H. E., Prata, A., Thordarson, T., and Carn, S.: Atmospheric processes affecting the separation of volcanic ash and SO<sub>2</sub> in volcanic eruptions: inferences from the May 2011 Grímsvötn eruption, *Atmos. Chem. Phys.*, 17, 10709–10732, <https://doi.org/10.5194/acp-17-10709-2017>, 2017.

925 Prata, A.T., Dacre, H.F., Irvine, E.A., Mathieu, E., Shine, K.P., Clarkson, R.J.: Calculating and communicating ensemble-based volcanic ash dosage and concentration risk for aviation. *Meteorol Appl.*, 26:253–266. <https://doi.org/10.1002/met.1759>, 2019.

930 Rémy, S., Kipling, Z., Flemming, J., Boucher, O., Nabat, P., Michou, M., Bozzo, A., Ades, M., Huijnen, V., Benedetti, A., Engelen, R., Peuch, V.-H., and Morcrette, J.-J.: Description and evaluation of the tropospheric aerosol scheme in the European Centre for Medium-Range Weather Forecasts (ECMWF) Integrated Forecasting System (IFS-AER, cycle 45R1), *Geosci. Model Dev.*, 12, 4627–4659, <https://doi.org/10.5194/gmd-12-4627-2019>, 2019.

935 Rix, M., Valks, P., Hao, N., Loyola, D., Schlager, H., Huntrieser, H., Flemming, J., Koehler, U., Schumann, U., and Inness, A.: Volcanic SO<sub>2</sub>, BrO and plume height estimations using GOME-2 satellite measurements during the eruption of Eyjafjallajökull in May 2010, *J. Geophys. Res.-Atmos.*, 117, D00U19, <https://doi.org/10.1029/2011JD016718>, 2012

940 Schmidt, A., et al. (2014), Assessing hazards to aviation from sulfur dioxide emitted by explosive Icelandic eruptions, *J. Geophys. Res. Atmos.*, 119, 14,180–14,196, doi:10.1002/2014JD022070.

945 Stohl, A., Prata, A. J., Eckhardt, S., Clarisse, L., Durant, A., Henne, S., Kristiansen, N. I., Minikin, A., Schumann, U., Seibert, P., Stebel, K., Thomas, H. E., Thorsteinsson, T., Tørseth, K., and Weinzierl, B.: Determination of time- and height-resolved volcanic ash emissions and their use for quantitative ash dispersion modeling: the 2010 Eyjafjallajökull eruption, *Atmos. Chem. Phys.*, 11, 4333–4351, <https://doi.org/10.5194/acp-11-4333-2011>, 2011.

950 Theys, N., Smedt, I. D., Yu, H., Danckaert, T., Gent, J. v., Hörmann, C., Wagner, T., Hedelt, P., Bauer, H., Romahn, F., et al.: Sulfur dioxide retrievals from TROPOMI onboard Sentinel-5 Precursor: algorithm theoretical basis., *Atmos. Meas. Tech.*, 10, <https://doi.org/10.5194/amt-10-119-2017>, 2017.

955 Thomas, H. E., and A. J. Prata (2011), Sulphur dioxide as a volcanic ash proxy during the April–May 2010 eruption of Eyjafjallajökull Volcano, Iceland, *Atmos. Chem. Phys.*, 11, 6871–6880, doi:10.5194/acp-11-6871-2011.

Tournigand, P.-Y., Cigala, V., Lasota, E., Hammouti, M., Clarisse, L., Brenot, H., Prata, F., Kirchengast, G., Steiner, A. K., and Biondi, R.: A multi-sensor satellite-based archive of the largest SO<sub>2</sub> volcanic eruptions since 2006, *Earth Syst. Sci. Data*, 12, 3139–3159, <https://doi.org/10.5194/essd-12-3139-2020>, 2020.

960 Vaughan, G., Wareing, D., and Ricketts, H.: Measurement Report: Lidar measurements of stratospheric aerosol following the 2019 Raikoke and Ulawun volcanic eruptions, *Atmos. Chem. Phys.*, 21, 5597–5604, <https://doi.org/10.5194/acp-21-5597-2021>, 2021.

Xu, J., Schüssler, O., Loyola R., D., Romahn, F., and Doicu, A.: A novel ozone profile shape retrieval using Full-Physics Inverse Learning Machine (FP-ILM), *IEEE J. Sel. Topics Appl. Earth Observ. Remote Sens.*, 10, 5442–5457, <https://doi.org/10.1109/JSTARS.2017.2740168>, 2017.

965 Yarwood, G., Rao, S., Yocke, M., and Whitten, G.: Updates to the carbon bond chemical mechanism: CB05, Final report to the US EPA, EPA Report Number: RT-0400675, available at: <http://www.camx.com> (last access: 18 May 2021), 2005.

